Pergamon

Journal of Structural Geology, Vol. 18, No. 12, pp. 1417 to 1435, 1996

PII: S0191-8141(96)00072-7
0191-8141/96 $15.00+0.00

# The tectonic significance of a porphyroblastic blueschist facies overprint during Alpine orogenesis: Sifnos, Aegean Sea, Greece

GORDON S. LISTER and ADAMANDIA RAOUZAIOS

Victorian Institute of Earth and Planetary Sciences, Department of Earth Sciences, Monash University, Melbourne 3168, Australia

(*Received* 17 *January* 1995; *accepted in revised form* 13 *August* 1996)

**Abstract**—The MacArgon program* has been used to model published $^{40}Ar/^{39}Ar$ apparent age spectra for white micas from the island of Sifnos, Cyclades, Greece. These micas formed during a period of porphyroblastic mineral growth ($M_2$) in the epidote–blueschist facies, at $> \sim 460$ °C and $< \sim 14$ kbar. $M_2$ marked the onset of a major period of deformation ($D_3$) during which kilometre-scale ductile shear zones formed and widespread recumbent folding took place. The modelling experiments suggest that flat apparent age spectra observed in the eclogite–blueschist domain (EBD) can only be obtained if the rocks cooled rapidly below ~350 °C after $M_2$ at ~42 Ma. Cooling rates must be > 50 °C/m.y., and since $M_2$ is followed by $D_3$ we infer that these are the cooling rates during $D_3$. Modelling experiments for micas from the greenschist domain (GSD) structurally underneath the EBD suggest that the GSD cooled rapidly, but at ~32 Ma. One tectonic model that might explain the rapidity of cooling rates inferred for the EBD model supposes that ambient temperatures were at ~500 °C when $M_2$ took place, but thereafter the high pressure rocks were thrust to the north and rapidly cooled as the result of their juxtaposition against cooler, shallower levels of the crust. Copyright © 1996 Elsevier Science Ltd

## INTRODUCTION

During the Eocene, high-pressure/low-temperature (HP–LT) metamorphism took place in the deep crustal roots of mountain belts formed by Alpine collisional orogenesis. In the Aegean the orogenic welt subsequently collapsed (Dewey 1988) and the mountain belt was torn apart by ongoing processes of continental extension. Eventually these high pressure metamorphic rocks were exposed at the surface, now as islands in the Aegean Sea. Sifnos (see Fig. 1) was chosen for detailed fabric and microstructural analysis because it is peripheral to the zone of metamorphic core complexes in the central Cyclades (Lister *et al.* 1984), and thus such a study would reveal more about the early history of collisional orogenesis in this part of the Alpine belt.

We can learn about the tectonic processes occurring during the destruction of mountain belts by tracking the history of high pressure rocks in space and time, and by combining information provided by structural geology, metamorphic petrology and geochronology. The application of this technique has proven useful in many different mountain belts in that it has allowed the large scale movement picture to be inferred (e.g. in the Pyrenees, Vissers 1992, the French Alps, Platt & Lister 1985, the Scandinavian Caledonides, Andersen *et al.* 1994, the Variscan orogeny, Diez Balda *et al.* 1995, or the Kigluaik Mountains, Alaska, Miller *et al.* 1992). Fabric and microstructural analysis allows the geologist to determine the mechanisms responsible for deformation, and the relative timing of deformation and metamorphism. Additional information provided by geochronology allows estimation of the absolute timing of different events, and the rates of the processes involved. The relation between deformation and metamorphism can then provide critical constraints for geodynamic models.

In many metamorphic terrains, study of the fabrics and microstructures has revealed that major episodes of metamorphism were closely followed by major episodes of deformation. For example in the Pyrenees, Zwart (1979), Vissers (1992) and Lister *et al.* (1986) observed that porphyroblasts that grew during LP–HT metamorphism have first overgrown pre-existing foliations statically (i.e. without accompanying deformation of the rock mass). However by the time that the last stages of

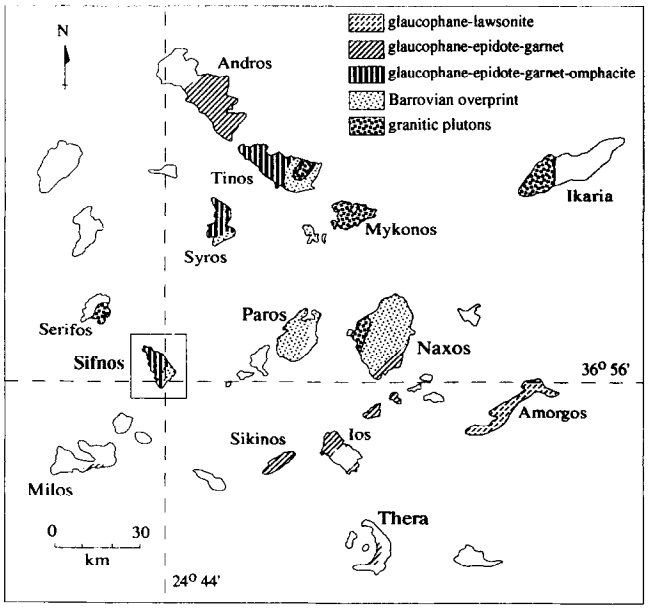


Fig. 1. A map of the Cyclades (modified from Ridley 1984), showing the location of Sifnos and the distribution of high-pressure mineral assemblages and Miocene granitic plutons.

*To obtain the most recent version of MacArgon go to WWW address: http://artemis.earth.monash.edu.au/MacArgon/.

growth took place, the inclusion trails in the porphyroblasts had begun to curve, indicating that deformation of the rock mass was taking place. Fabrics and microstructures in the rock surrounding the porphyroblasts show that this period of deformation continued, and in some shear zones high strains then accumulated (e.g. Vissers 1992). It is suggested that these metamorphic events have initiated as the result of a wave of heat and/or fluid propagating upwards through the metamorphic pile, and that the mechanical weakening that results in consequence thereof may have allowed the initiation of a major period of tectonism. In this paper we discuss an example where such a sequence of events appears to have taken place during high pressure–low temperature metamorphism, on the island of Sifnos in the western Cyclades.

There have been many different studies conducted on Sifnos, including $^{40}Ar/^{39}Ar$ geochronology (Wijbrans *et al.* 1990), detailed metamorphic petrology (Okrusch *et al.* 1978, Schliestedt 1986) and several estimates of *P–T* conditions using mineral geochemistry (Matthews & Schliestedt 1984, Evans 1986, Schliestedt & Matthews 1987, Avigad *et al.* 1992). These have provided valuable information on the work described in this paper. A period of epidote–blueschist facies blastic mineral growth overprints a jadeite- and omphacite-bearing foliation on Sifnos, and we are interested in the geodynamic significance of this event. Fabric and microstructural analysis (Raouzaios 1993) links the timing of this growth event into the sequence of structural events observed on Sifnos. Metamorphic petrology provides some constraint on the conditions during this growth event, and on the *P–T* path subsequently followed by these rocks.

First we summarize available data in relation to the relative timing of deformation and metamorphism. After discussing the existing geochronology, in particular the $^{40}Ar/^{39}Ar$ geochronology carried out by Wijbrans *et al.* (1990), we then model the effect of different *P–T–t* histories proposed in the literature. We can predict the apparent age spectra that would result from published *P–T–t* paths by using the MacArgon program (see Lister & Baldwin in press). However these *P–T–t* paths do not allow explanation of the published $^{40}Ar/^{39}Ar$ apparent age spectra. Finally we use a technique we call parametric inversion to define a range of *P–T–t* paths that result in apparent age spectra similar to those measured from Sifnos. This information offers an important constraint on the nature of the tectonic processes that might have operated.

## GEOLOGY OF SIFNOS

Sifnos is an island in the western Cyclades (see Fig. 1) on which strongly deformed and metamorphosed sedimentary and volcanic rocks crop out (Davis 1966). The stratigraphic sequence is commonly divided into four main lithological units (e.g. as in Okrusch *et al.* 1978, Matthews & Schliestedt 1984, Schliestedt & Matthews 1987). The distribution of these four units is shown in Fig. 2 and a brief description of each is given below, in order of structurally lowest to highest:

(1) The *greenschist unit* occurs at the base of the pile and is exposed mainly in the central and southeastern part of the island. It consists of retrograde albite–epidote–blueschist and greenschist facies schists and gneisses, with occasional marble intercalations up to a few tens of meters thick.

(2) The *main marble unit* structurally overlies the greenschist unit and occupies most of central and southern Sifnos. It is mainly composed of grey and white calcite marble with a few rather distinct horizons of dolomitic marble. Locally, the marble grades into calc-schists containing greenschist facies minerals such as chlorite, epidote, white mica and actinolite. Intercalations of metavolcanic rocks are also contained within the sequence. These are up to 100 m thick and are generally now greenschists. However outcrops with relatively well preserved blueschist assemblages are also found within this unit, in particular, at the southernmost part of the island, and to the northwest of the small bay south of Kamares.

(3) The *blueschist unit* is exposed in the north of the island and overlies the main marble unit. It contains spectacular outcrops of well preserved eclogite and blueschist facies schists and gneisses. Metabasic gneisses

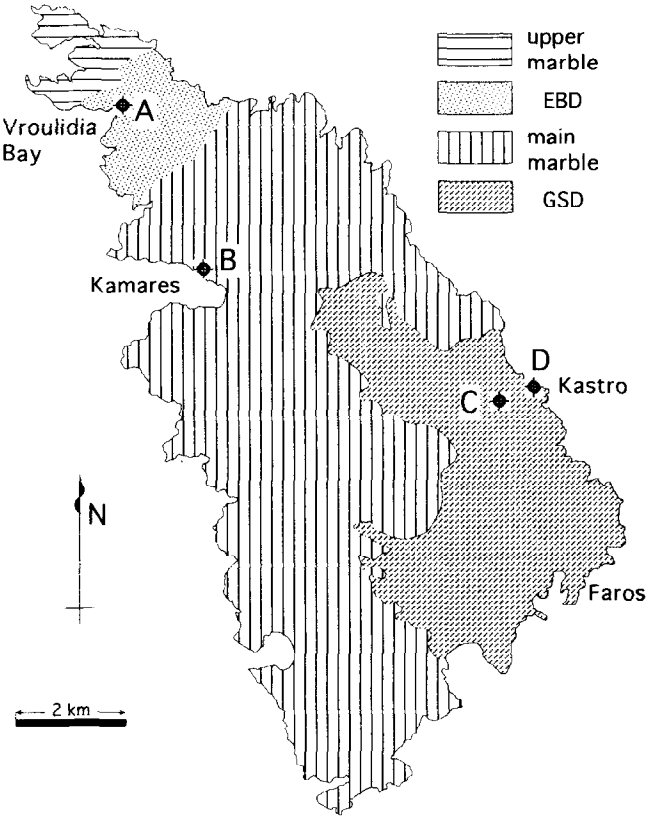


Fig. 2. Geological map of Sifnos (modified after Davis 1966), showing the exposures of the eclogite–blueschist domain (EBD), the greenschist domain (GSD) and the marble units. Also shown are the locations of the geochronology samples used by Wijbrans *et al.* (1990) which have been referred to in this paper.

include omphacite-rich layers with porphyroblastic garnet, glaucophane and epidote and abundant glaucophane-rich layers with porphyroblastic garnet, white mica and epidote. Meta-acidic rocks have quartz- and jadeite-rich assemblages with porphyroblasts of garnet and glaucophane. All of these assemblages contain white mica which has crystallised as porphyroblasts in some rocks and defines a foliation in others. Several intercalations of metapelites and quartzites also occur within the eclogite–blueschist domain.

(4) The *upper marble unit* overlies the blueschist unit and occupies the northernmost part of the island. It consists mainly of grey and white calcite marbles with a few dolomitic and schist horizons. The schists in the upper marbles appear similar to those of the underlying eclogite–blueschist domain, although they are not as well preserved.

In this paper the two main schist horizons are divided into separate structural and metamorphic domains. These will be referred to as the eclogite–blueschist domain (or the EBD) and the greenschist domain (or the GSD). The outcrop of these two domains is shown in Fig. 2.

The obvious differences in the metamorphic history of the rocks of the two schist horizons have been interpreted in various ways. Earlier workers (Matthews & Schliestedt 1984, Schliestedt & Matthews 1987) suggested that the greenschist facies transformation was caused by pervasive upward flowing fluids, and that these fluids did not reach the eclogite–blueschist domain because the main marble unit behaved as an impermeable layer. More recent workers (Avigad & Garfunkel 1991, Avigad 1993) suggested that a low angle tectonic contact exists between the two domains, and propose that the GSD has undergone a regional, Barrovian, greenschist facies overprint prior to being juxtaposed against the overlying main marble unit late in the tectonic history. The EBD then escaped retrogression because it had been uplifted to shallow crustal levels prior to the time of juxtaposition. The EBD and the GSD may have followed significantly different $P$–$T$–$t$ paths if the nature of the contact between the GSD and the overlying marbles (and hence the EBD) is tectonic in origin. The timing of juxtaposition of the two units has yet to be resolved however.

## STRUCTURE AND METAMORPHISM

The rocks of Sifnos have been intensely deformed and most of the original sedimentary and igneous textures obliterated. The planarity of bedding on the outcrop scale is in most cases due to stretching during deformation, and the apparent simplicity of lithological layering can be deceptive. Zones of intense isoclinal folding are not uncommon and four generations of deformation have been recognized (Raouzaios 1993) in both the EBD and the GSD. There is sparse evidence for $D_1$ and the existence of this deformation is based on the observation of $S_1$ as inclusion trails in occasional garnet porphyroblasts and on the fact that $S_2$ is differentiated. The $S_1$ inclusion trails are defined by glaucophane, epidote, quartz and mica and we infer that $D_1$ took place under blueschist facies conditions.

$D_2$ formed an intense foliation, and this differentiated crenulation cleavage ($S_2$) is pervasively developed over the island. In the EBD, adjacent grains of jadeite and quartz were aligned in $S_2$ and stably co-existed. Omphacite needles (also aligned in $S_2$) occur as stable inclusions in garnet. These observations indicate that $D_2$ took place at the high pressures of the eclogite facies, but at relatively low temperatures. The $D_3$ deformation involved the formation of major ductile shear zones in which an intense NE trending $L_3$ mineral lineation is developed. During $D_3$, earlier formed fabrics were stretched and strongly disrupted, and $D_3$ is responsible for the exhumation of the rock mass to $P$–$T$ conditions at which the assemblage jadeite + quartz is unstable. $D_4$ involved the formation of recumbent folds, and NW trending mineral lineations. $S_4$ has commonly developed in the hinge zones of $F_4$ folds in the GSD but is rare in the EBD. $D_4$ occurred at $P$–$T$ conditions within the glaucophane stability field. Both $D_3$ and $D_4$ involved the production of 1–1000 m scale recumbent folds.

There was a major period of static mineral growth ($M_2$) subsequent to $D_2$, and this continued through the early stages of $D_3$ (Raouzaios 1993). Glaucophane has developed grain-boundary microstructures dominated by effects related to the minimization of surface-free energy (Vernon 1976). Micas (paragonite and phengite) are invariably decussate. Large porphyroblasts of glaucophane (0.1–4.0 cm), epidote (0.5–5.0 cm), garnet (1.0–3.0 cm), paragonite (0.1–0.5 cm) and phengite (0.1–1.0 cm) grew (often euhedrally) over the $S_2$ cleavage. In many cases porphyroblasts have straight inclusion trails that are seemingly continuous with $S_2$ in the external matrix. In some cases $S_2$ cleavage septa can be recognized in inclusion trails, and these may curve into a more intensively deformed external $S_2$ foliation. These microstructures imply blastic mineral growth before and during the early stages of $D_3$, prior to the development of intense $D_3$ fabrics. Further $D_3$ deformation caused progressive reorientation of large $M_2$ epidote laths and glaucophane needles into the plane of $S_3$.

Porphyroblastic mica can readily be recognized in outcrop and in thin section. In thin section the micas develop decussate textures, and grow in different orientations with respect to $S_2$. Growth and recrystallization of mica during $M_2$ is so prevalent that it seems reasonable to assume that previous $^{40}Ar/^{39}Ar$ geochronological studies (Altherr *et al.* 1979, Wijbrans *et al.* 1990) measured apparent age spectra that reflect the effect of conditions subsequent to $M_2$. However, even though most mica appears to have grown during the $M_2$ event, the effects of subsequent deformations can still be recognized, since the $M_2$ micas are folded, kinked, disrupted and shredded, with sliding and/or splitting on the (0001) cleavage plane leading to reduction of the thickness of individual grains. Some mica recrystallization has occurred during $D_3$ and $D_4$, for example in cleavage septa and along microshears.

In the GSD there has been extensive new mica growth during the $M_3$ episode of mineral growth, which occurs subsequent to $D_3$ and prior to $D_4$.

## CONDITIONS OF METAMORPHISM

Matthews & Schliestedt (1984) and Schliestedt & Matthews (1987) concluded that two metamorphic events affected the rocks of Sifnos: an initial prograde eclogite–blueschist facies metamorphism that was followed by a retrogressive greenschist facies overprint. However, microstructural analysis carried out by Raouzaios (1993) showed that several distinct periods of metamorphic mineral growth took place throughout this history. These growth episodes can be assigned to different $P$–$T$ fields, and are used to constrain $P$–$T$–$t$ paths used to simulate the development of $^{40}Ar/^{39}Ar$ apparent age spectra in this paper. The mineral parageneses and metamorphic facies definitions of Evans (1990) have been adopted.

### *Conditions of metamorphism in the eclogite–blueschist domain*

Two major periods of metamorphic mineral growth affect the rocks of the eclogite–blueschist domain. Early mineral growth ($M_1$) took place during prograde regional metamorphism in which $P$–$T$ conditions passed through the lawsonite blueschist facies and peaked at eclogite–blueschist facies. Although lawsonite is no longer preserved in the assemblages of Sifnos, its existence prior to the peak metamorphism was detected by Okrusch *et al.* (1978), who identified box shaped inclusions in garnet as pseudomorphs of clinozoisite and white mica after lawsonite. Thus lawsonite was present during garnet growth but was obliterated once temperatures exceeded 450 °C. The EBD assemblages contain either jadeite + quartz or omphacite + garnet accompanied by the typical blueschist facies minerals glaucophane, epidote and white mica. $P$–$T$ conditions during peak metamorphism ($M_1$) have been estimated at 470–520 °C and 14–18 kbar from garnet–omphacite geothermometry (Schliestedt 1986), the stability of the assemblage jadeite + quartz (Okrusch *et al.* 1978) and the reaction of deerite–magnetite–riebeckite to grunerite–magnetite–quartz (Evans 1986).

The porphyroblasts which grew during the $M_2$ episode (garnet, glaucophane, epidote and white mica) overprint $S_2$ fabrics and define a paragenesis representative of the epidote–blueschist facies. Microstructural analysis does not reveal any new growth of the eclogite facies pyroxenes jadeite and omphacite during $M_2$. However, the equilibrium textures of $S_2$ aligned omphacite and jadeite inclusions in $M_2$ garnet porphyroblasts suggest that $M_2$ began near eclogite facies conditions. The extensive growth of garnet during $M_2$ provides a lower temperature limit of 460 °C (Okrusch *et al.* 1978). An upper pressure limit is provided by the breakdown of deerite (see previous paragraph for reaction) which was calculated as occurring at a pressure of 14 kbar for a temperature of 450 °C (Evans 1986). This upper pressure limit is in agreement with the stability field of $M_1$ jadeite ($Jd_{90}$) + quartz which becomes unstable during $M_2$ and develops rims of albite and acmitic pyroxene (Okrusch *et al.* 1978). In addition, the reaction of omphacite and garnet or white mica to form glaucophane and epidote suggests that the boundary between eclogite facies and epidote–blueschist facies conditions was crossed during this growth event.

Curved $S_2$ inclusion trails in garnet porphyroblasts from several locations indicate that $M_2$ growth continued through to the early stages of $D_3$. This suggests that $D_3$ began at $P$–$T$ conditions similar to those of $M_2$. There is complete breakdown of jadeite + quartz to albite in zones of intense $D_3$ strain (measured by Schliestedt 1986, with a jadeite content of $\sim 50$ %), and omphacite is observed to become unstable in $D_3$ shear bands. This indicates that pressures of $\sim 11$ kbar were reached during $D_3$. Hence the pressure range for $D_3$ spans 11–14 kbar, suggesting that a significant degree of tectonic exhumation is associated with this event.

Mineral growth subsequent to $M_2$ is limited to rocks that have undergone substantial $D_3$ and $D_4$ strain. This suggests that temperatures were too low to drive reactions without deformation enhanced diffusion (e.g. as the result of fluid ingress into active ductile shear zones). The $P$–$T$ conditions during the latest deformation are difficult to constrain because of limited and widely varied mineral growth. In $D_4$ shear zones chlorite replaces garnet and omphacite breaks down but glaucophane remains stable. Therefore an upper pressure limit is provided by the omphacite stability field and a lower pressure limit is provided by the glaucophane stability field. Thus the pressure range during $D_4$ can loosely be constrained to within 6–11 kbar (for the temperature range 300–400 °C).

### *Conditions of metamorphism in the GSD*

The GSD consists of greenschist and epidote–blueschist facies rocks with some minor intercalation of partially preserved eclogite facies rocks. Petrographic observations indicate that the higher grade assemblages of the GSD are related to the lower grade assemblages by a series of hydration and carbonation reactions (Avigad *et al.* 1992). These reactions are dependent on the availability of fluids and are not restricted to rocks of particular bulk compositions. Microstructural analysis has identified three episodes of retrograde metamorphism subsequent to the peak prograde eclogite facies event ($M_1$). The $P$–$T$ conditions of $M_1$ in the GSD have been assumed to be similar to those of the eclogite–blueschist domain due to the presence of relict omphacite and garnet assemblages (Altherr *et al.* 1979, Matthews & Schliestedt 1984, Evans 1986, Schliestedt & Matthews 1987, Wijbrans *et al.* 1990).

The first phase of retrograde mineral growth ($M_2$) involves overprinting of earlier assemblages by the epidote–blueschist facies minerals: garnet, glaucophane,

epidote, paragonite, phengite and albite. This is a similar mineral paragenesis to that of $M_2$ for the eclogite–blueschist domain, except that albite porphyroblasts are much more common in the GSD and garnet porphyroblasts occur to a considerably lesser extent. The albite porphyroblasts form from the breakdown of both jadeite and omphacite indicating that the GSD was at crustal levels below 12 kbar during $M_2$.

The second phase of retrogression ($M_3$) occurs near the epidote–blueschist and greenschist facies boundary and involves static overprinting of $D_3$ fabrics. $M_3$ involved the growth of epidote, white mica, albite and sphene and the recrystallization of glaucophane, albite and white mica. Glaucophane grains develop heterogeneous compositions in response to changing chemical and $P$–$T$ conditions and often formed actinolitic and/or crossitic rims. Evidence that this metamorphism occurs near greenschist facies conditions is provided by the replacement of garnet by chlorite, and chlorite growth in $S_3$ crenulation cleavages and shear bands.

Temperature estimates using oxygen isotope geothermometry have produced a range of 370–490 °C for overprinted assemblages of the GSD (Matthews & Schliestedt 1984). The measurements form two clusters about 440–490 °C and 370–380 °C. These estimates are obtained from quartz–epidote and quartz–phengite mineral pairs and may represent mineral equilibration during $M_2$ or $M_3$. Calculations carried out by Avigad *et al.* 1992 (using the THERMOCALC software, Holland & Powell 1985, Powell & Holland 1988, and the GEOCALC PTX software, Berman & Perkins 1987, Berman 1988) for epidote–blueschist facies assemblages (including glaucophane, albite, chlorite, paragonite and muscovite) give a pressure range of 8–10 kbar at an assumed temperature of 450 °C. This is in agreement with similar calculations carried out by Schliestedt & Matthews (1987). Since chlorite growth is associated with $M_3$ (and not $M_2$) this pressure range of 8–10 kbar is thought to be more representative of $M_3$.

Subsequent to $D_4$ the final period of retrogression ($M_4$) occurs under greenschist facies conditions suggesting that pervasive fluid infiltration during $M_4$ did not occur. Where $M_4$ retrogression has taken place, there has been extensive growth of chlorite, albite, epidote, calcite, actinolite, sphene and magnetite and the complete breakdown of garnet and glaucophane. In the zones affected by $M_4$, glaucophane is completely replaced by chlorite and actinolite suggesting that it is well out of its stability field. Calculations (made by Avigad *et al.* 1992) using the THERMOCALC software for the equilibration of a greenschist facies assemblage containing actinolite, albite, chlorite, epidote and muscovite gave a pressure of 5.5 kbar at an assumed temperature of 450 °C.

### *Comparison of P–T conditions in the EBD and GSD*

Mineral growth associated with the $M_2$ porphyroblastic event indicates higher pressures in the eclogite–blueschist domain and possibly higher temperatures also. These higher pressures are indicated by the preservation of jadeite in the EBD, whereas in the GSD jadeite breaks down completely (during $M_2$) to form albite porphyroblasts. The extensive blastic growth of garnet in the EBD, compared to a significantly lesser degree of garnet growth in the GSD, may indicate slightly higher temperatures for the EBD during $M_2$. In the GSD, $M_3$ is a major metamorphic episode which statically overprints intense $D_3$ fabrics and structures whereas in the EBD, post-$M_2$ mineral growth is limited to zones which have undergone substantial $D_3$ and $D_4$ strain. The difference in the degree of $M_3$ metamorphism between the two domains suggests either that temperatures were higher in the GSD at this time and/or that more fluids were available to allow reactions to proceed towards equilibrium.

The pressure estimate for the GSD during $M_3$ (8–10 kbar) places the GSD at a similar level in the crust to the EBD during the period following $D_3$. If, in fact the EBD was deeper than the GSD during $M_1$ and $M_2$ then the similar pressures these domains experience during $M_3$ suggests uplift of the eclogite–blueschist domain relative to the GSD either prior to or during $M_3$. Since $D_3$ is the only deformation which has been recognized between $M_2$ and $M_3$, the proposed relative uplift of the eclogite–blueschist domain must have occurred during the $D_3$ event. Our favoured hypothesis is that the eclogite–blueschist domain was thrust over the GSD during $D_3$.

The GSD has experienced substantial greenschist facies retrogression during $M_4$. This final period of metamorphism largely involves the replacement of high pressure phases by chlorite and has affected those parts of the GSD that were infiltrated by fluids. The eclogite–blueschist domain largely escaped this episode of metamorphism because fluids did not infiltrate it. Avigad (1993) suggest that the GSD underwent greenschist facies retrogression at 5.5 kbar when the eclogite–blueschist domain was at shallow crustal levels ($< 10$ km). However, their evidence is not conclusive and the two domains may have been at similar crustal levels during $M_4$.

## GEOCHRONOLOGY

There have been a number of geochronological studies on Sifnos. Altherr *et al.* (1979) reported the results of Rb–Sr, K–Ar, and fission track studies. They obtained (dominantly 3T) phengites from the best preserved high pressure rocks in the eclogite–blueschist domain, and found that these micas produced almost concordant Rb–Sr and K–Ar ages ($\sim$42 Ma). Less preserved high pressure assemblages yielded $2M_1$ and 3T phengites. These gave K–Ar ages in the range 41–48 Ma, whereas Rb–Sr ages on the same minerals fell in the range 37–33 Ma. The older K–Ar ages were interpreted as being the result of the incorporation of excess argon in the samples. Altherr *et al.* (1979) separated $2M_1$ phengites from the greenschist domain that yielded Rb–Sr and K–Ar ages in the range 21–24 Ma, and interpreted these ages as representing the effects of the greenschist facies

metamorphism that overprinted the earlier high pressure metamorphic rocks.

Sphene from an eclogite in northern Sifnos yielded a fission track age of ~15 Ma. Gleadow & Lovering (1978) suggest that this implies cooling below 270 °C by 15 Ma for a cooling rate of ~20 °C/m.y. There is considerable uncertainty attached to the interpretation of fission track ages in sphene however. Direct dating of sphene from the German KTB deep drill hole suggests that at least some sphene may retain fission tracks to significantly higher temperatures (Coyle *et al.* 1994). There is also evidence of considerable variation in annealing properties between different sphenes, probably due to compositional differences. Sphene from high pressure metamorphic rocks is likely to demonstrate significant differences from sphene in granites, on which most laboratory annealing studies have been conducted (e.g. Naeser & Faul 1969, Gleadow 1978). Altherr *et al.* (1982) measured apatite fission track ages from the island of Serifos, immediately to the north of Sifnos, and obtained a cooling age of ~8 Ma, suggesting that final exhumation of the metamorphic rocks to pressures ~2 kbar and temperatures <120 °C had occurred by about this time.

In this paper we have modelled published $^{40}Ar/^{39}Ar$ apparent age spectra measured by Wijbrans *et al.* (1990) using laser step-heating on single flakes of phengitic white mica. These authors reported a total of 11 step-heating experiments, four from the schists and gneisses of the EBD, three from the schists of the main marble unit, and four from the underlying GSD. The age spectra obtained from white micas in the eclogite–blueschist domain were relatively flat, and Wijbrans *et al.* (1990) reported that "in none of the cases was a gradual increase of apparent ages noted". The apparent age ranged from 36–42 Ma (e.g. Fig. 3a). However, in samples from the schist horizon in the main marble unit, apparent ages step up in the first few percent of gas release from 17–24 Ma to well-defined (and relatively flat) plateaux in the age range 32–36 Ma (e.g. Fig. 3b). In the greenschist domain of Sifnos, relatively flat apparent age spectra were also obtained, with plateaux in the range 30–32 Ma. These apparent age spectra show the effect of significant argon loss, with the initial gas fraction (up to 10–12 % release) displaying apparent ages ranging from 0–28 Ma (Fig. 3c). One sample yielded a flat spectrum with a plateau age of ~19 Ma (Fig. 3d). Note that the term 'plateau age' has been used loosely here, in the sense that the apparent age spectra have a number of relatively well-defined segments that cluster about a particular value.

Raouzaios *et al.* (1996) reported preliminary results of an $^{40}Ar/^{39}Ar$ geochronological study from Sifnos that suggests even more complexity than apparent above. For the EBD it is possible to correlate apparent age with the fabrics and microstructures observed in thin section. Recrystallization and grain growth in intensely deformed samples resulted in lower apparent ages, more representative of later deformation events. These lower ages and more disrupted spectra are not observed from lesser deformed samples, such as those measured by Wijbrans *et al.* (1990).

At this stage we cannot indicate to what extent the apparent age spectra obtained by Wijbrans *et al.* (1990) are representative of the different tectonic units as a whole. For example, to date there has been only one sample measured on Sifnos (by Wijbrans *et al.* 1990) that recorded a Miocene plateau age. We suspect that this is because the effects of the $M_4$ event (i.e. the late stage greenschist facies retrogression) are rather more localized within the greenschist domain than might have been expected.

## MODELLING $^{40}Ar/^{39}Ar$ APPARENT AGE SPECTRA

To interpret $^{40}Ar/^{39}Ar$ apparent age spectra in a more quantitative fashion we have to assume that there is a certain amount of useful information encapsulated in the shape of an apparent age spectrum. If the apparent age spectra do contain useful information, this can be extracted by carrying out a study such as the one we report, where a detailed study of the fabrics and microstructures, correlated with the metamorphic evolution of the tectonites concerned, is combined with a detailed geochronological study. In this paper, to simulate the development of apparent age spectra in phengite, it has been assumed that argon accumulates in the mineral grain as the result of the radioactive decay of $^{40}K$, and that argon is lost to the ambient pore fluid solely as the result of solid state volume diffusion. In addition, it has been assumed that the release of argon into the vacuum during the measurement process (in this case laser step-heating experiments of single grains in a vacuum) also takes place as the result of solid-state volume diffusion. This implies that the shape of the apparent age spectra reflects concentration gradients of $^{40}Ar^*$ within the diffusion domains, and that processes such as dehydroxylation of the mica during the measurement process do not obscure detail in the apparent age spectra. These assumptions remain a point of contention. Solid-state volume diffusion is not the only process responsible for argon loss in nature and in the experimental apparatus.

### *Limitations of the technique*

The critical aspect is the behaviour of phengite under vacuum during step-heating experiments. Dehydroxylation will destroy the mica structure, so there is no guarantee that the shape of the apparent age spectrum that results from step heating experiments represents effects related to the internal concentration gradient of $^{40}Ar^*$ within individual diffusion domains. Apparent age spectra obtained from hydrous phases such as hornblende, biotite and muscovite may simply reflect progress of the breakdown process (e.g. Lee *et al.* 1991). There is a definite dependence on the step-heating schedule in such circumstances. Effects such as degassing fluid inclusions may also play an important role. Thus although the shape of apparent age spectra obtained from phengite might resemble those obtained from the theoretical

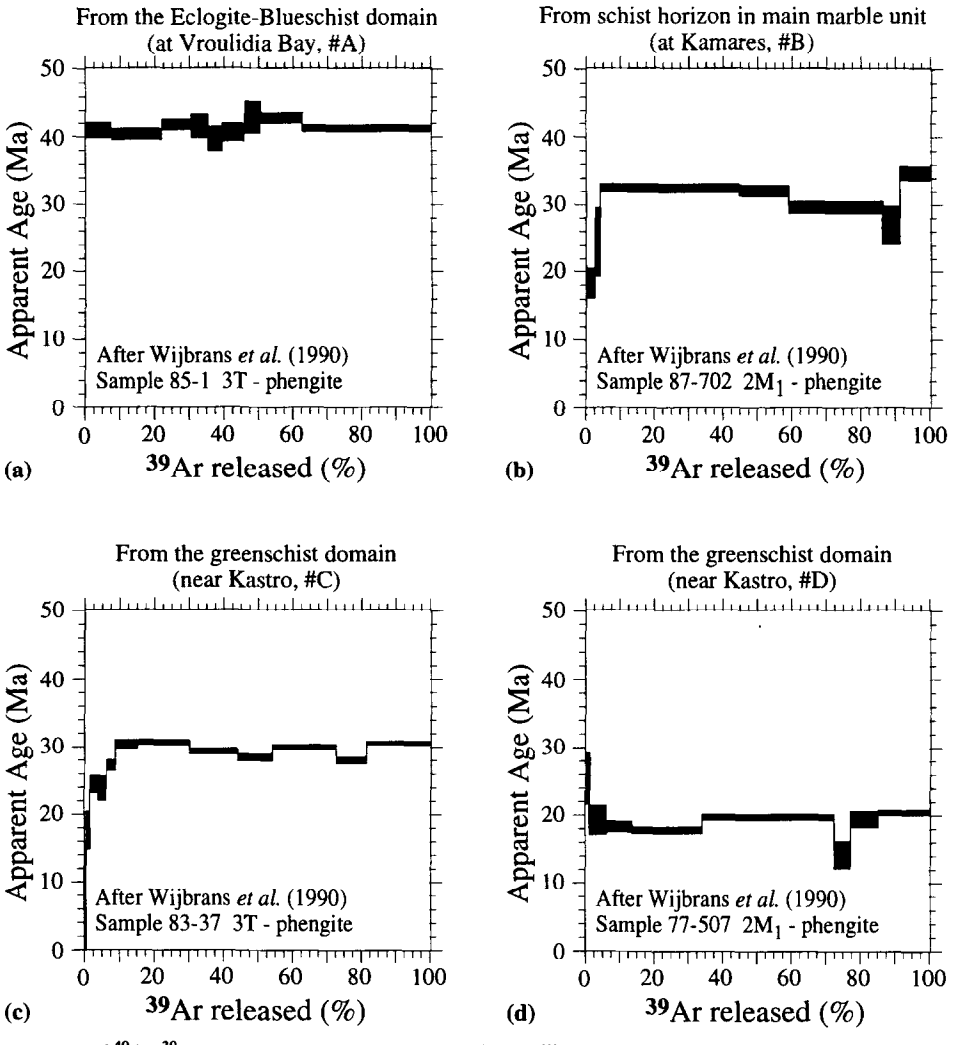


Fig. 3. Examples of $^{40}Ar/^{39}Ar$ apparent age spectra measured by Wijbrans *et al.* (1990) using laser step-heating experiments on phengitic white micas from Sifnos: (a) sample 85-1 *(location #A)* from the EBD showing a 'flat' spectrum; (b) sample 87-702 *(location #B)* from the main schist layer in the main marble unit showing minor partial argon loss, with a plateau age of ~32 Ma; (c) sample 83-37 *(location #C)* from the GSD showing the effects of partial argon loss, with a plateau age of ~30 Ma; and (d) sample 77-507 *(location #D)* also from the GSD showing a flat apparent age spectrum due to a Miocene greenschist facies overprint. Locations of samples are shown in Fig. 2.

simulations, this in itself is not sufficient to show that solid-state volume diffusion has been the mechanism that has allowed release of argon during the step-heating experiments.

However, the shape of the spectra that have been obtained by Wijbrans *et al.* (1990) do resemble those that would be produced during step heating of single diffusion domains as the result of solid state volume diffusion. Moreover Wijbrans *et al.* (1990) did obtain consistent apparent age spectra from within each structural and metamorphic domain on Sifnos. Within the EBD, the various apparent age spectra measured show no signs of argon loss (e.g. Fig. 3a). Within the GSD the variation of apparent age spectra is typical of the effects of partial loss (e.g. Fig. 3c). The resemblance between actual and theoretical apparent age spectra obtained from phengite is striking, and this provides sufficient justification for the attempt at a more quantitative approach to the interpretation of apparent age spectra adopted in this paper. We accept that future research may show this attempt to have been unjustified.

### *Modelling the development of $^{40}Ar/^{39}Ar$ apparent age spectra with MacArgon*

If it is assumed that the $^{40}Ar/^{39}Ar$ apparent age spectra measured on Sifnos reflect solid-state volume diffusion, flat spectra such as obtained from the eclogite–blueschist domain imply that: (a) there was rapid cooling through the closure temperature; (b) generally low ambient temperatures applied since the time that the micas crystallized or recrystallized; and/or (c) the rocks have not been subjected to a significant thermal pulse since the time at which the micas closed and/or recrystallized. Similarly, stepped age spectra of the type reported from the greenschist domain can be interpreted as the result of partial loss of argon, either: (a) as the result of slow cooling through the closure temperature; (b) as the result of relatively high ambient temperatures (see Lister & Baldwin in press); or (c) during a thermal pulse. If such conclusions can be drawn they have some relevance to the question of providing constraint on the types of *P–T–t* path that could have been followed by the rocks on

Sifnos. Therefore we have simulated the effect of different *P–T–t* paths proposed for the rocks on Sifnos using the MacArgon program (see Lister & Baldwin in press).

We used version 4.00 of the MacArgon program (see Lister & Baldwin in press) to simulate the effect of arbitrarily chosen *P–T–t* histories on $^{40}Ar/^{39}Ar$ age spectra. The program requires as input: (a) a set of diffusion parameters (as above); (b) an exactly specified pressure–temperature–time (*P–T–t*) history. Once a simulation has been performed the apparent age spectra can be determined using the MacSpectrometer. If the proposed *P–T–t* paths produce similar apparent age spectra to those measured on Sifnos, then the predicted *P–T–t* paths might match the actual history of the rock. If the predicted apparent age spectra are significantly different from those observed, then either the proposed *P–T–t* path is inappropriate, or the basic assumptions made in performing the simulations are false.

Argon diffusion in a mineral grain can be predicted if we use the basic relation for diffusivity D:

$$D = D_0 \exp[-(Q + P\bar{v})/RT]$$

as long as the following parameters are known: $Q$, the activation energy for diffusion; $\bar{v}$, the activation volume; $D_0$, the frequency factor; the geometry of the diffusion domain (either a sphere, slab, or a cylinder); and $\mu$, the appropriate radius or half-thickness of the diffusion domain (e.g. see McDougall & Harrison 1988). However, there are no experimental data as to the retentivity of argon in phengite. Wijbrans & McDougall (1986, 1988) assumed that the experimental data for phlogopite (Giletti 1974) might act as a reasonable approximation. We have followed their lead and used this data in our MacArgon simulations.

The diffusion parameters for phlogopite were obtained by Giletti (1974) as the result of a sequence of hydrothermal experiments. From these experiments the following parameters were obtained, assuming cylindrical diffusion domains:

$Q = 57.9$ kcal mol$^{-1}$

$D_0 = 0.75$ cm$^2$/s

$\mu = 150\ \mu$m

$\bar{v} = 10$ cm$^3$ mol$^{-1}$

Using these parameters to estimate the closure temperature, at 10 kbar, for a cooling rate of 50 °C/m.y., closure in phlogopite will occur at 459 °C. For a cooling rate of 5 °C/m.y., at 10 kbar, closure will occur at 422 °C. However, Wijbrans *et al.* (1993) assumed a closure temperature of 360 °C for phengite, and this choice is apparently incompatible with the above diffusion data.

We have therefore illustrated some simulations using muscovite diffusion data. Lister & Baldwin (in press) reanalysed available diffusion data from Robbins (1972) and propose a slab geometry for muscovite, with the following diffusion parameters:

$Q = 41.8$ kcal mol$^{-1}$

$D_0 = 3.352 \times 10^{-7}$ cm$^2$/s

$\mu = 5.9\ \mu$m

$\bar{v} = 10$ cm$^3$ mol$^{-1}$ (assumed as a first approximation)

Using the above diffusion data for muscovite, at zero pressure, closure at ~360 °C would require cooling rates of ~19 °C/m.y. At 10 kbar, closure at 360 °C would require a cooling rate of 2.6 °C/m.y. Wijbrans *et al.* (1993) cool the EBD at ~10 °C/m.y. and the GSD at ~5.6 °C/m.y. At cooling rates appropriate for the EBD, using muscovite diffusion parameters, closure would occur in the range 349–384 °C, for pressures 0–10 kbar. For the GSD, closure would occur in the range 339–373 °C, for pressures 0–10 kbar. Thus we can obtain estimates of closure temperature broadly consistent with the models advocated by Wijbrans *et al.* (1993), at least in terms of the cooling rates predicted by their models, but only by assuming that the diffusion parameters appropriate to muscovite apply.

Note that the experimental diffusion data for muscovite support a slab geometry (see Lister & Baldwin in press), and there is no *a priori* reason to assume that diffusion in a sheet silicate should behave more like a cylindrical model. The diffusion parameters for phlogopite rather than muscovite have been used in the majority of the simulations because these parameters define the most retentive model mineral. For comparison, some simulations have been performed with diffusion parameters appropriate to muscovite, which is much less retentive. If the parameters appropriate for muscovite were used in these calculations, predicted rates of cooling would be higher, and the ambient temperatures to which we suggest the rock mass must have cooled would be considerably lower.

To compare our results with observed apparent age spectra we have ignored the information contained in the first 5 % of gas release in the MacSpectrometer, after a MacArgon simulation. A potential source of ambiguity arises in that relatively small volumes of gas are released with the laser technique applied to single mica grains, and this obscures information that otherwise might be available in the early gas release fraction. In one case Wijbrans *et al.* (1990) note "a large gas release in the first step... obscures any fine structure" in the apparent age spectra. Since most of the information regarding the cooling history of a mineral is found in the first 10–20 % of gas released, a large fraction of gas release in the first step will obscure this information. If the gas step is large enough, the apparent age spectrum can appear flat whereas it would have been stepped if smaller gas fractions had been measured. This is not a significant problem because most of the apparent age spectra measured by Wijbrans *et al.* (1990) contain a considerable amount of detail. However if we ignore a greater fraction of the initial gas release in the MacSpectrometer

(e.g. up to 10%) then few constraints are offered by this type of analysis as to the nature of the *P–T–t* paths followed by the rocks on Sifnos.

## PUBLISHED *P–T* TRAJECTORIES AND SIMULATED APPARENT AGE SPECTRA

Different *P–T–t* paths have been proposed for the Sifnos rocks by previous authors (Matthews & Schliestedt 1984, Wijbrans *et al.* 1990,1993). We use these *P–T–t* paths as input to the MacArgon program and predict the $^{40}Ar/^{39}Ar$ apparent age spectra that would result.

The first of these we consider is the classic Alpine loop proposed for Sifnos by Matthews & Schliestedt (1984). This *P–T* loop (Fig. 4a) involves high pressure metamorphism followed by isothermal decompression until Miocene greenschist facies retrogression takes place. The exact form of the *P–T–t* history used in the simulations is shown in Fig. 4(b). The results of the simulations are shown in Fig. 4(c) (for the phlogopite model) and Fig. 4(d) (for the muscovite model). This *P–T–t* path involves an approximately isothermal drop in temperature from 500 °C to 450 °C while decompression takes place from 14 kbar to 5 kbar.

With such a *P–T–t* history, closure in the mica grains takes place only after Miocene greenschist retrogression is complete. Relatively young apparent ages are obtained from the simulations, because mica held at ~450 °C for several million years will retain no memory of the older high pressure event. Old apparent ages will not be obtained using such a *P–T–t* loop. Thus the classic

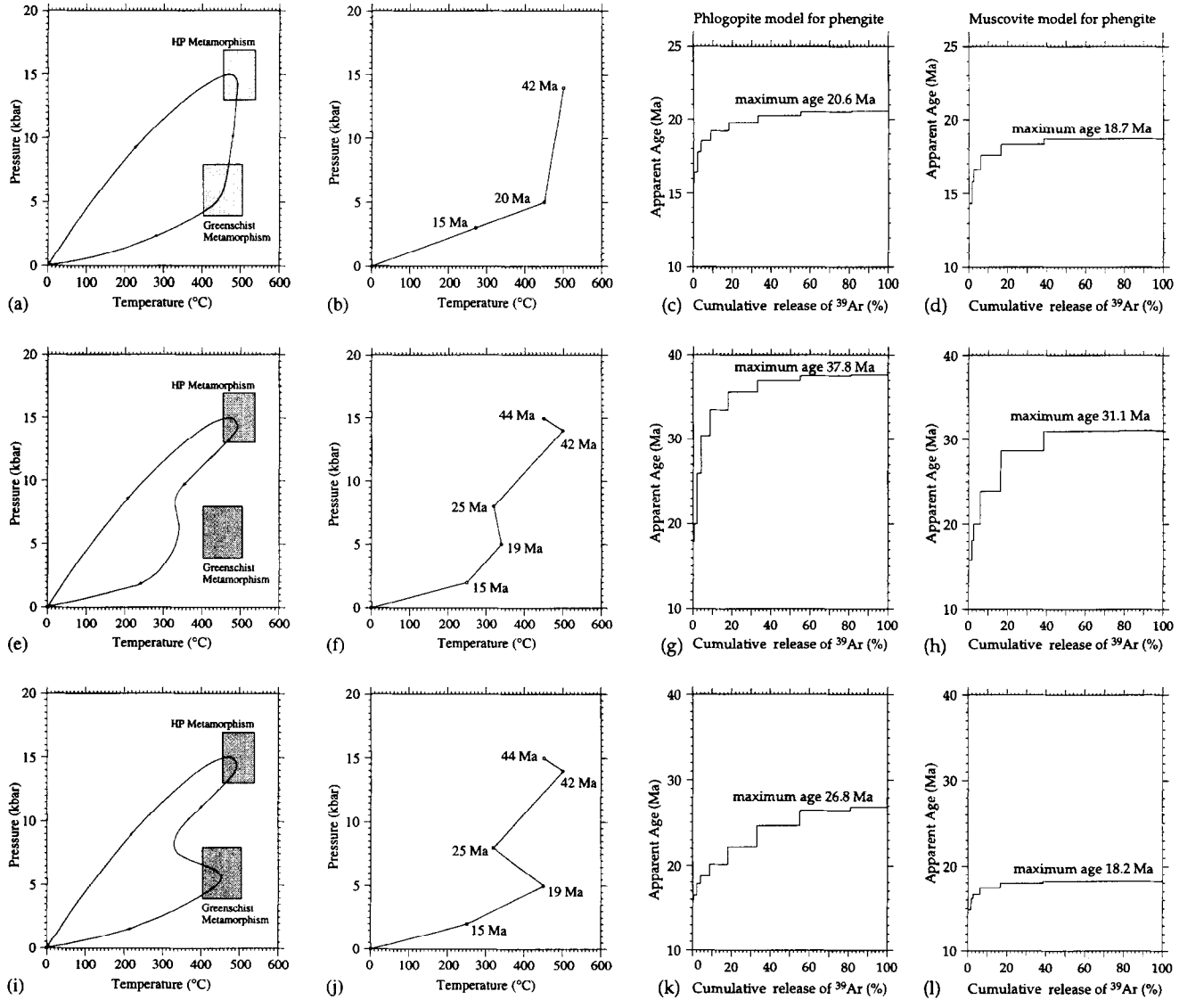


Fig. 4. Different *P–T* trajectories (a, e and i) discussed by Wijbrans *et al.* (1990) are used to construct *P–T–t* paths (b, f and j) for input to the MacArgon program. Apparent age spectra are produced by the MacSpectrometer (c, d, g, h, k and l). Diffusion parameters appropriate to phlogopite were used in one case (c, g and k) and diffusion parameters appropriate to muscovite in the other (d, h and l). (a) Classic Alpine *P–T* loop proposed by Matthews & Schliestedt (1984). (e) *P–T* trajectory proposed by Wijbrans *et al.* (1990) for the EBD. (i) *P–T–t* trajectory proposed for the GSD has a Miocene thermal pulse responsible for the greenschist facies overprint. The simulated spectra are significantly different from the measured spectra, suggesting that the *P–T–t* trajectories proposed by Wijbrans *et al.* (1990) may be inappropriate.

Alpine *P–T* path proposed by Matthews & Schliestedt (1984) is inconsistent with the geochronological data obtained by Wijbrans *et al.* (1990).

To avoid this difficulty Wijbrans *et al.* (1990) suggested a significant modification of the *P–T* trajectories that must be followed by the Sifnos rocks (see Figs. 4e & i). The *P–T* trajectory followed by the GSD involves a thermal excursion during the Miocene (Fig. 4i), whereas in the EBD the effects of this thermal excursion are not observed (Fig. 4e). Figures 4(f) and (j) show the actual *P–T–t* histories used to imitate the *P–T* trajectories proposed by Wijbrans *et al.* (1990) for simulations using the MacArgon program. The apparent age spectra that result from the simulations are shown in Figs. 4(g) and (k) (for phlogopite) and in Figs. 4(h) and (l) (for muscovite).

These particular *P–T–t* histories allow the EBD to remain above ~450 °C for several million years, so the predicted apparent age spectra reflect the effect of cooling from this period. The apparent age spectra predicted for the EBD using the *P–T–t* history shown in Fig. 4(f) has a ~38 Ma plateau for the phlogopite model (Fig. 4g) and a ~31 Ma plateau for the muscovite model (Fig. 4h). Significant partial loss of argon has taken place in both cases, so that stepped apparent age spectra result. However, apparent age spectra measured in the EBD on Sifnos have plateau ages at ~40–42 Ma, and there is no evidence of such a degree of argon loss in the actual measured spectra (e.g. compare the simulated spectra with Fig. 3a). To explain the data for the EBD on Sifnos we will show that *P–T–t* paths input into the MacArgon program have to involve rapid cooling from about ~40–42 Ma. Otherwise, significant partial loss of argon is observed in the simulated spectra. Hence we can eliminate *P–T–t* paths that imply slow cooling in the EBD.

The apparent age spectra obtained for the GSD, using the *P–T–t* history in Fig. 4(j), have plateau ages at ~27 Ma and ~18 Ma for the phlogopite and muscovite models, respectively. We are therefore unable to replicate the relatively old apparent ages measured in the GSD by Wijbrans *et al.* (1990) using these *P–T–t* paths. In addition, although both the measured and simulated apparent age spectra from the GSD have a shape indicative of significant partial argon loss, the measured spectra reflect considerably less partial argon loss (compare Fig. 3c with Figs. 4k & l). Thus *P–T–t* paths as illustrated in Fig. 4(j) are not consistent with the available geochronological data from the GSD.

## *P–T–t* TRAJECTORIES CALCULATED USING GEODYNAMIC MODELS

Wijbrans *et al.* (1993) developed a quantitative geodynamic model for the evolution of Sifnos, and predicted the actual *P–T–t* trajectories that would be followed by different rock units (see Figs. 5a & e). They concluded that exhumation of blueschist facies rocks such as those exposed on Sifnos "must take place within 5–10 km of the active subduction zone to preserve blueschists and eclogites". The subducting slab provides a cooling mechanism, preventing an increase of the geothermal gradient during uplift, which would otherwise retrograde the rocks under greenschist facies conditions. Uplift of the high pressure rocks is proposed to be buoyancy driven and requires reversal of movement along detachment faults that form parallel to the subduction zone system to enable material to be returned to the surface.

The *P–T–t* histories produced by the Wijbrans *et al.* (1993) geodynamic model (Figs. 5a & e) have also been used as input to the MacArgon program, allowing us to estimate their effect on $^{40}Ar/^{39}Ar$ apparent age spectra. Figures 5(b) and (f) show the input *P–T–t* trajectories. The shapes of the apparent age spectra that result are shown in Figs. 5(c) and (g) (for phlogopite) and Figs. 5(d) and (h) (for muscovite). For the case in which phlogopite diffusion data are used (see Figs. 5c & g) the MacArgon simulations predict older plateau ages than have been measured. These older ages result because phlogopite is more retentive of argon than muscovite, under identical conditions. If the muscovite diffusion data are used, as in Figs. 5(g) and (h), the MacArgon simulations predict plateau ages that are compatible with those measured in the EBD, but for the GSD the predicted plateau age is 10 m.y. younger than that observed. In comparison to the measured spectra (Fig. 3) all of the simulated $^{40}Ar/^{39}Ar$ spectra in Fig. 5 show a much greater degree of partial argon loss than is observed. Thus the *P–T–t* trajectories that result from the geodynamic model of Wijbrans *et al.* (1993) are not consistent with the measured apparent age spectra.

## PARAMETRIC INVERSION OF THE MEASURED APPARENT AGE SPECTRA

There is a discrepancy between the apparent age spectra that have been predicted using MacArgon simulations based on published *P–T–t* paths in comparison with the apparent age spectra that have actually been measured on Sifnos. The next step therefore was to use the MacArgon program to constrain the range of *P–T–t* paths that are capable of producing apparent age spectra that match the measured spectra (see Fig. 3). To do this we adopted a parametric approach.

Parametric inversion is accomplished in the following way. Two *P–T–t* paths are chosen that are substantially different, one from the other, in some essential ingredient. These are end-members, and we consider a range of *P–T–t* paths that vary from one end-member to the other. The computer works out each possible *P–T–t* path by performing a linear combination of the two paths specified above as end members. The computation begins with one end member *P–T–t* path ($\zeta = 0.0$), and then increments the linear combination factor, $\zeta$, until the final calculation is performed for the other end member *P–T–t* path ($\zeta = 1.0$). This is described by variation of the linear combination factor, $z$, in the range 0–1. We can then vary the parameters that describe a *P–T–t* history until we obtain reasonable matching of the apparent age

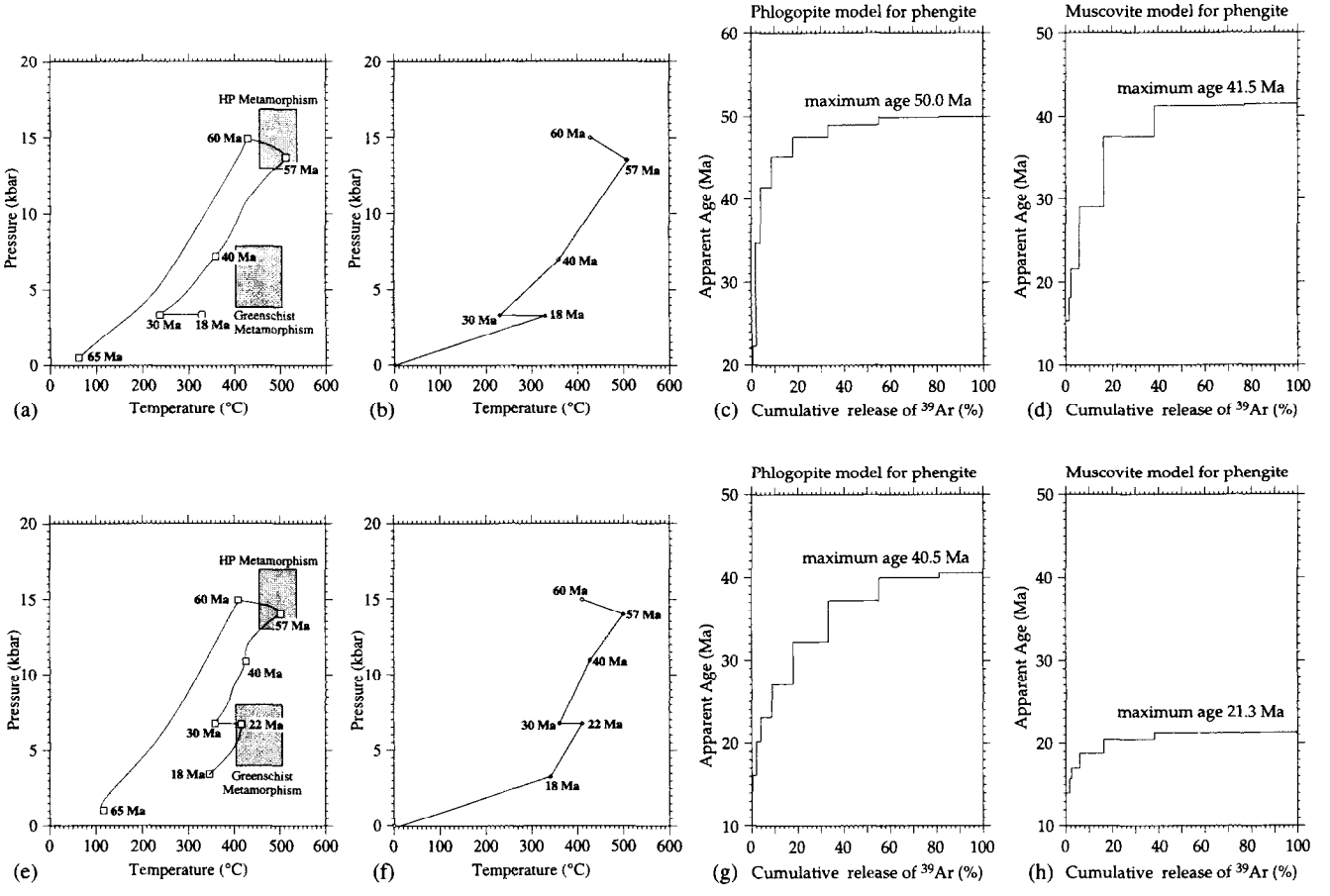


Fig. 5. (a) *P–T–t* trajectories predicted by the geodynamic model of Wijbrans *et al.* (1993) for the EBD; (e) *P–T–t* trajectory predicted for the GSD; (b) and (f) actual *P–T–t* trajectories used to simulate the development of $^{40}Ar/^{39}Ar$ apparent age spectra based on the geodynamic model; (c) and (g) produced using the diffusion parameters for phlogopite; (d) and (h) produced using the diffusion parameters for muscovite. The simulated spectra are significantly different from the measured spectra (see Fig. 3), since they display the effects of significant partial argon loss.

spectra produced in the MacSpectrometer in comparison with the actual measured apparent age spectra. In this way we can define a range of parameters that produces apparent age spectra that are compatible with those actually measured from Sifnos.

*MacArgon models for the eclogite–blueschist domain*

For the purposes of this paper, one-dimensional parameterization has been performed. Figure 6(a) shows a range of *P–T–t* paths that vary essentially only in the initial rate of cooling. By allowing a range of cooling rates we can observe the effect of this variable on the shape of the apparent age spectra. Thus we can constrain the range of cooling rates that produce relatively flat apparent age spectra. The estimated conditions for $M_2$ are chosen for the starting point since microstructural observations allow us to infer either growth or recrystallization of white mica during the $M_2$ event. Thus the first pinning point is set at 500 °C and 14 kbar. A range of paths is then considered which cool at different rates from this pinning point to a temperature of 300 °C. The most rapid rate considered is 200 °C m.y.$^{-1}$ and the slowest is 8 °C m.y.$^{-1}$. During this time, pressure is also decreased by an appropriate amount. For example in the case of the most rapid cooling (200 °C m.y.$^{-1}$) the pressure does not drop at all, whereas in the case of the slowest cooling rate (8 °C m.y.$^{-1}$), the pressure drops to 5 kbar. The second pinning point (120 °C, 2.5 kbar, 8 Ma) is based on apatite fission track ages obtained for Serifos (for location of this island see Fig. 1). We chose this pinning point because we assume that the rocks of Sifnos were also uplifted to similarly shallow depths at this time. Subsequent to the second pinning point all paths assume a common *P–T–t* path to the surface (see Fig. 6a).

This simple exercise accomplishes a great deal, because in doing these calculations, we have covered the broad range of possible *P–T–t* paths constrained by our detailed fabric and microstructural investigations. Paths outside of this range, such as the *P–T–t* trajectories in Figs. 4 and 5, are not considered here because they have already been shown to produce apparent age spectra that are incompatible with the measured spectra of Wijbrans *et al.* (1990). If we examine the apparent age spectra produced as the result of assuming diffusion parameters

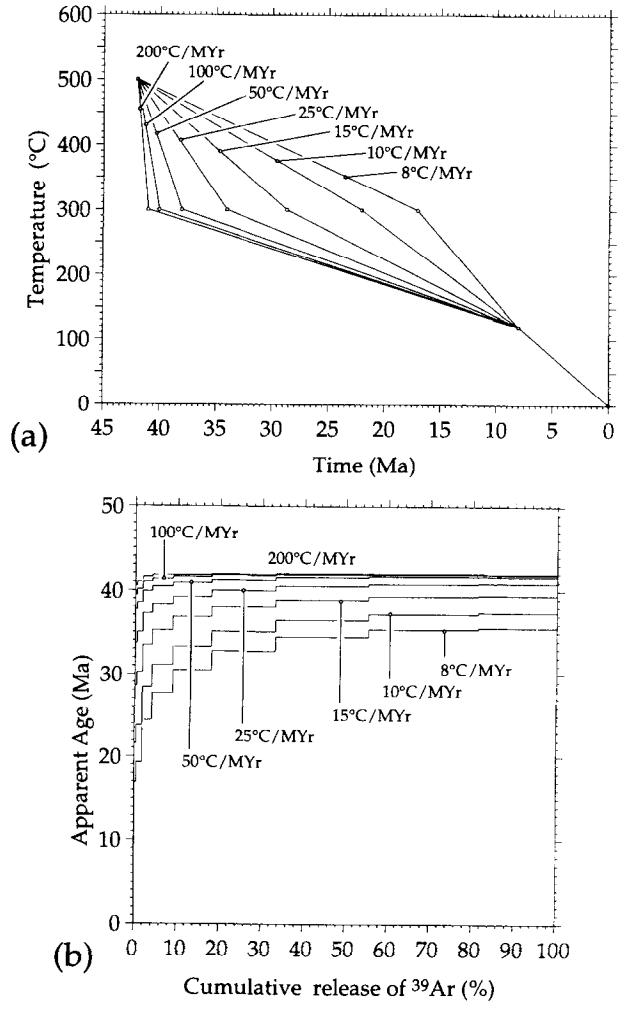


Fig. 6. Parameterization of the effect of cooling rate on the $^{40}Ar/^{39}Ar$ apparent age spectra for phlogopite. (a) *P–T–t* histories used in the simulations begin at (500 °C, 14 kbar, 42 Ma) then cool to 300 °C. From there the paths continue at a different but constant cooling rate to (120 °C, 2.5 kbar, 8 Ma), and thence to the surface. (b) Synoptic plot of apparent age spectra from each trajectory. Flat spectra are produced if cooling rates exceed ~50 °C m.y.$^{-1}$

appropriate to phlogopite (Fig. 6b), it can be seen that *P–T–t* paths that involve rapid cooling (> 50 °C m.y.$^{-1}$) result in apparent age spectra that have a minimal degree of partial argon loss, and they exhibit flat plateaux. Thus as the result of this single parameterization we have considerably reduced the number of options available for further constraint of the types of *P–T–t* paths possible. The choice of muscovite diffusion parameters (instead of phlogopite) would require rapid cooling (at > 50 °C m.y.$^{-1}$) to temperatures < 300 °C. We conclude that the flat shape of the argon spectra from the EBD suggests that an initially rapid drop in temperature occurs after $M_2$ blastesis.

The next variable parameter we consider (see Fig. 7) is aimed at determining to what temperatures the rocks must cool during this period of rapid temperature decrease. To ascertain this variable we used the following strategy. All *P–T–t* paths start at 500 °C and 14 kbar (as before), and then cool to 270 °C and 5 kbar. However, for one end member *P–T–t* path considered ($\zeta = 0.0$) the rate of cooling is rapid, but it remains constant only until 450 °C is reached. Then the rate of cooling dramatically slows. For the other end member *P–T–t* path ($\zeta = 1.0$) the rate of cooling is rapid, and rapid cooling continues at a constant until 270 °C is reached. Then temperature is kept constant until 15 Ma, while pressure slowly decreases. From 15 Ma all *P–T–t* paths involve rapid cooling.

This range of *P–T–t* paths allows an estimate of the minimum temperature to which the rocks must rapidly cool before slower cooling commences. Flat spectra will always be preserved if the rocks rapidly cool to 270 °C, at 100 °C m.y.$^{-1}$, as shown in Fig. 7(a) (for $\zeta = 1.0$). The range of *T–t* paths used for initial cooling at a rate of 100 °C m.y.$^{-1}$ is shown (Fig. 7a), as well as the resultant apparent age spectra (Fig. 7b). The apparent age spectra that result are quite flat as long as temperature decreases below ~350 °C before slower cooling commences (i.e., within the shaded area in Fig. 7a).

This result is assessed by varying the rate of initial rapid cooling. Figure 7(c) shows *T–t* paths with initial cooling rates equal to 50 °C m.y.$^{-1}$ These result in apparent age spectra that are still quite flat, but there is an increased degree of partial argon loss. Again, significant partial argon loss can be prevented as long as rapid cooling continues until < ~350 °C (Fig. 7d). Figure 7(e) shows *T–t* paths when the rate of cooling is initially 25 °C m.y.$^{-1}$. Figure 7(f) shows the apparent age spectra that result. There is now quite a noticeable degree of partial argon loss. It can therefore be concluded that in simulations for the EBD (see Fig. 7) relatively flat apparent age spectra will result only if there is rapid cooling after the $M_2$ event at a rate > 50 °C m.y.$^{-1}$ to temperatures lower than ~350 °C.

*MacArgon models for the greenschist domain*

We have also considered (see Fig. 8) the types of *P–T–t* paths that would produce $^{40}Ar/^{39}Ar$ apparent age spectra as observed by Wijbrans *et al.* (1990) from the GSD. As an example, Fig. 3(c) illustrates the apparent age spectrum measured from a 3T phengite separated from a sample taken from the GSD near Kastro (location #C, Fig. 2). This sample shows evidence of minor argon loss in the first 5–10 % of gas release. To produce such an effect the *P–T–t* history must include rapid cooling at ~32 Ma, otherwise the relatively flat plateau that is present cannot be replicated. It is also necessary to assume rapid cooling to < ~350 °C to preserve relatively flat plateaux in the apparent age spectra, and to remain below this temperature for the remainder of the geological history. Such a *P–T–t* path is shown in Fig. 8(a) ($\zeta = 0.0$). This *P–T–t* path involves rapid cooling from 460 °C and 9 kbar, at 32 Ma, to 350 °C and 7 kbar, at 30 Ma. Thereafter temperatures and pressures linearly decrease until 8 Ma at 120 °C and 2.5 kbar (using the constraint offered by apatite fission track measurements from Serifos).

An added complication in the GSD is that a thermal pulse may have taken place in the Miocene. The single apparent age spectrum from the GSD that produced a

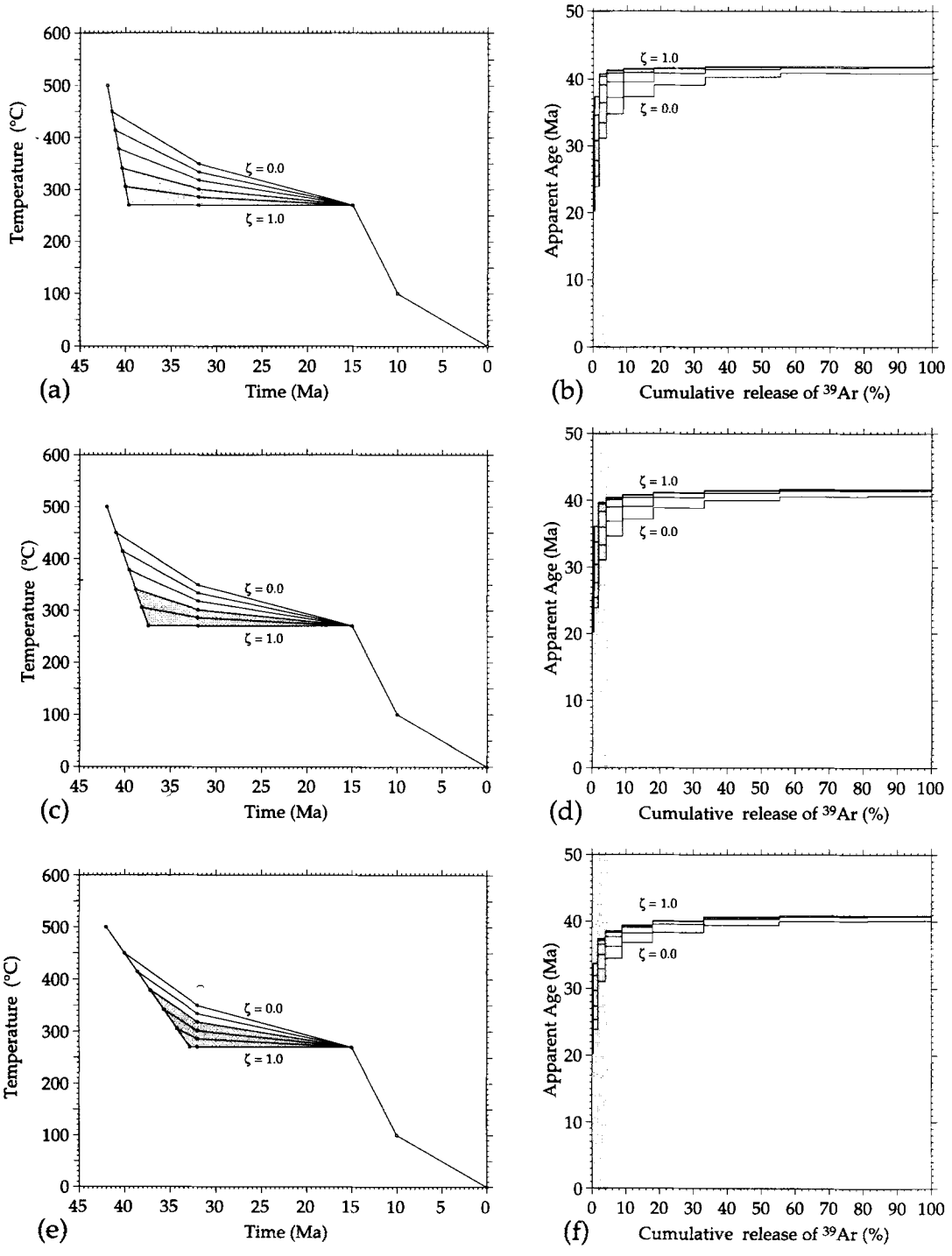


Fig. 7. Parameterization of the effect of the magnitude of temperature decrease during rapid cooling after $M_2$: (a), (c) and (e) *P–T–t* paths cooling from (500 °C, 14 kbar, 42 Ma) at 100 °C m.y.$^{-1}$, 50 °C m.y.$^{-1}$ and 25 °C m.y.$^{-1}$ respectively. One end member *P–T–t* path drops the temperature to only 450 °C before slow cooling commences (i.e. $\zeta = 0.0$). This *P–T–t* path always results in considerable argon loss. The other end member *P–T–t* path drops the temperature to 270 °C and then isothermal decompression commences (i.e. $\zeta = 1.0$). This type of path minimises the amount of partial argon loss and produces relatively flat apparent age spectra. In (a), (c) and (e) the shaded area represents the *P–T–t* paths which produce apparent age spectra similar to those for the $\zeta = 1.0$ trajectory; (b), (d) and (f) show the apparent age spectra that would result (assuming diffusion data appropriate to phlogopite).

Miocene plateau age (Fig. 3d) has a relatively flat plateau, which could be the result of recrystallization during a Miocene thermal pulse and rapid cooling thereafter. A Miocene thermal pulse was thus considered as part of the parametric study. This is illustrated in Fig. 8.

The effect of the Miocene thermal pulse was simulated by allowing an immediate temperature increase (to as high as 500 °C) at 20 Ma, and then linear cooling over the next 2 m.y. If the temperature during the Miocene pulse exceeds 450 °C for at least 0.5 m.y. ($\zeta = 1.0$) there will be little argon retained in the model phlogopite. To allow preservation of the older ages, without the effects of greatly increased partial argon loss, peak temperatures during the Miocene thermal pulse must not exceed 350 °C over a period $< 2$ m.y. (i.e., $\zeta$ in the range 0.0–0.4, shaded area in Fig. 8). It can therefore be concluded that the

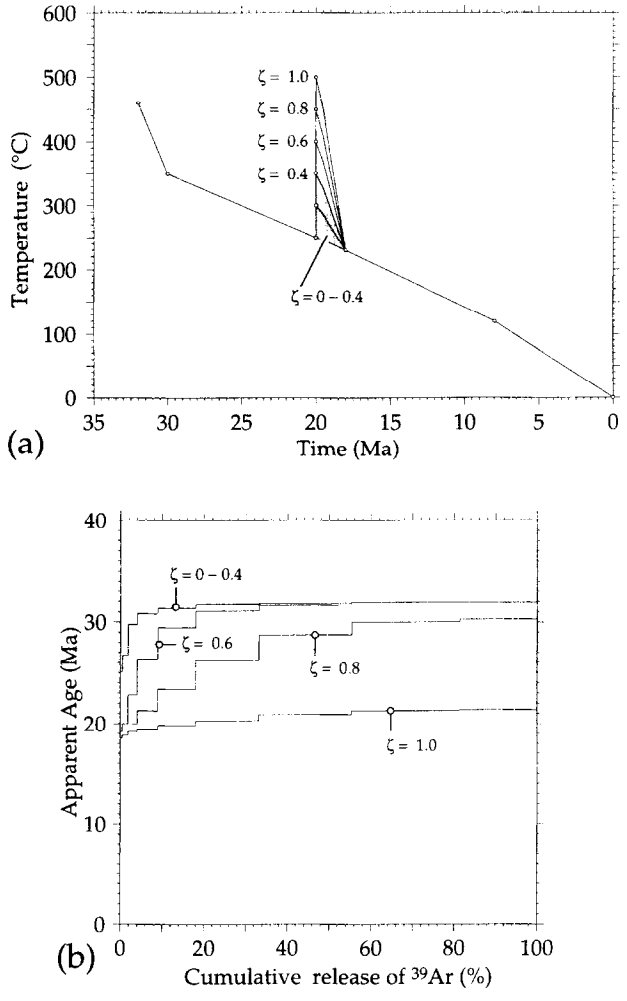


Fig. 8. Parametric modelling of the effects of a Miocene thermal pulse on the apparent age spectra observed from the GSD. (a) *P–T–t* histories used in the simulations. (b) Simulated apparent age spectra (assuming diffusion data appropriate to phlogopite). The *P–T–t* trajectory for $\zeta = 0.0$ involves no Miocene heating and produces apparent age spectra which match those measured by Wijbrans *et al.* (1990) from the GSD. The *P–T–t* trajectory for $\zeta = 1.0$ includes a thermal pulse at 20 Ma which reaches a peak temperature of 500 °C and then cools rapidly to $<250$ °C m.y.$^{-1}$ by 18 Ma. This produces a relatively flat spectrum with a plateau age of ~21 Ma. The range of *P–T–t* trajectories from $\zeta = 0.0$ to $\zeta = 0.4$ will produce spectra that are not affected by the Miocene thermal pulse. Thus this parametric study shows that a Miocene thermal pulse must be of short duration ($< \sim 2$ m.y.) with temperature $<350$ °C.

effects of the Miocene event are only of local significance throughout much of the GSD. Otherwise younger ages would be prevalent.

## DISCUSSION

The results above are important for two different reasons. First there is a clear implication in our interpretation of the apparent age spectra that rapid cooling in the EBD has taken place from ~450 °C to $< \sim 350$ °C over a period less than ~3 m.y. in duration. Second we imply that, thereafter, temperatures in the EBD slowly decreased from 350 °C for the remainder of the geological history. Brief excursions above these ambient temperatures cannot be ruled out, but the duration of any subsequent thermal pulse must be short. Continued cooling is not necessary if the rocks initially cool rapidly to $< \sim 300$ °C.

### *Tectonic implications of rapid cooling at depth in the Earth's crust*

The central issue is to explain how rapid cooling to such low ambient temperatures can be achieved at relatively deep levels in the continental crust. Our main conclusion is that if ambient temperatures of ~500 °C at 50 km (~14 kbar) were applicable prior to the $M_2$ event (as would be the case for a geothermal gradient of ~10 °C km$^{-1}$) it would be difficult to drop temperatures rapidly to 350 °C after the $M_2$ event. However such rapid cooling is possible as the result of tectonic activity, if this is assumed to have taken place at a rate that was relatively fast (e.g. $>8$ cm y$^{-1}$ convergence, see below).

Rapid cooling can take place if rocks at depth are juxtaposed against cooler rocks as the result of the operation of lithospheric scale thrusts or extensional detachments. Thrusting of deep crustal levels over shallower cooler rocks will lead to rapid cooling of the overthrust sheet of rock, at a rate depending on the consequent temperature differences that are created. Conversely, crustal scale extensional shear zones or detachments exhume rocks from great depth and juxtapose these deeper level rocks against rocks from relatively cool surficial levels. In this case, rapid cooling takes place in the lower plate.

The action of a large scale low-angle normal (detachment) fault can be illustrated using the thermal model of Voorhoeve & Houseman (1988). An initial lithospheric thickness of 140 km is assumed and a crustal thickness of 70 km. If the initial geotherm is 10 °C km$^{-1}$, a temperature of 500 °C is achieved at ~14 kbar. The detachment is assumed to dip at 30°, and an instantaneous relative displacement of 80 km is allowed to take place. Figure 9 shows how the geotherm will evolve over the first 2.5 m.y. after such an event. Such a radical solution will allow the rocks to cool rapidly below 300–350 °C, but such rates of cooling are only achieved in the immediate vicinity of the detachment surface. However this model requires instantaneous decompression from 14 kbar to 3 kbar, so it is incompatible with the available *P–T* estimates for metamorphic conditions along the decompression path. Therefore this cannot be the explanation for the period of rapid cooling that has been inferred on Sifnos.

At such great depths, for the time scales we consider, it is possible to ignore conditions at the surface (including factors such as erosion or tectonic denudation) since these will cause only second order effects at depth. Therefore the model of Voorhoeve & Houseman (1988) was modified to allow prediction of cooling rates after lithospheric scale thrusting. Again a crustal thickness of 70 km is assumed, and a lithospheric thickness of 140 km. A geothermal gradient of 10 °C km$^{-1}$ is used, and we examine the evolution of the crustal geotherm after an instantaneous thrust event has taken place. An instantaneous relative displacement of 80 km creates a 400 °C temperature step across the thrust. Figure 10(a) shows

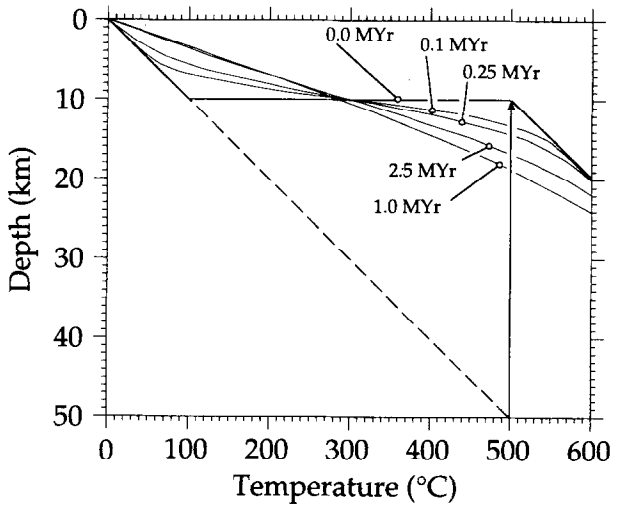


Fig. 9. Temperature–depth history after instantaneous relative displacement on an extensional detachment fault, illustrating the evolution of the crustal geotherm with time (after Voorhoeve & Houseman 1992), for a crustal profile in which the detachment is intersected at 10 km. Continental crust 70 km thick has been moved 80 km on a 30 ° dipping detachment fault. We assume a 10 °C km$^{-1}$ geothermal gradient, and a lithosphere thickness of 140 km. Temperatures decrease below 350 °C within 2 m.y., up to 5 km distant from the detachment. However, considerable depressurization is implied by such an event, if cooling below 350 °C is to be accomplished.

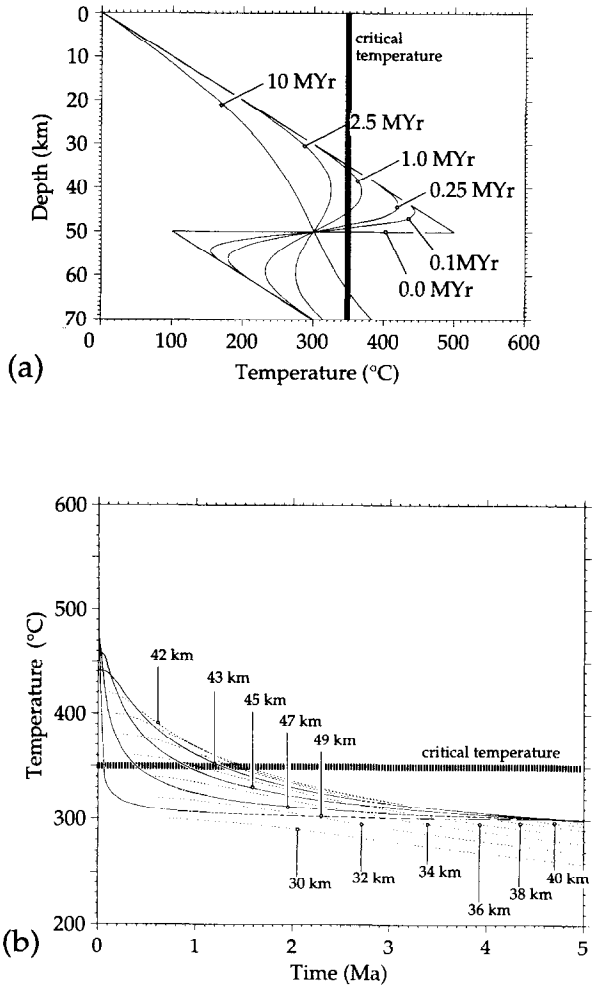


Fig. 10. (a) Temperature–depth plots after instantaneous overthrusting, illustrating the evolution of the crustal geotherm for a crustal profile in which the thrust plane is intersected at 50 km. Continental crust 60 km thick has been overthrust 80 km, on a 30° dipping thrust plane. The effects of erosion have not been taken into account. We assume a 10 °C km$^{-1}$ geothermal gradient, and a lithosphere thickness of 140 km. (b) The temperature–time history at different crustal depths up to 1–20 km distant from the thrust plane. Temperatures decrease below 350 °C within 2 m.y. of the onset of thrusting. The dotted lines are temperature–time profiles for rocks at shallow depths, where the rate of cooling is no longer so rapid.

the evolution of the crustal geotherm and Fig. 10(b) shows the temperature–time paths for different levels in the crust above the thrust. Rapid cooling occurs in the upper-plate, even up to 10 km distant from the thrust plane. After 25 m.y., the geotherm has decreased to half of its initial value. Thereafter (but this is not shown on the diagram) if the lithospheric thickness and basal temperature remained the same, the geotherm would very slowly have begun to rise towards its initial value.

Figure 10(b) shows the time–temperature evolution at a number of specific crustal depths, up to 20 km distant above the thrust plane. Temperatures would be driven rapidly below 300–350 °C in the immediate vicinity of the fault plane because the temperature step across such a thrust is quickly relaxed by conduction of heat from the upper plate to the lower plate. Rapid cooling occurs up to 10 km away from the thrust plane, with temperatures dropping below 350 °C within 2 m.y. Thrust movements on the lithospheric or crustal scale are thus capable of explaining the period of rapid cooling inferred for Sifnos. Of course a relative displacement of 80 km on such a thrust plane could not be achieved instantaneously. Nevertheless, if such a relative displacement was achieved over a relatively short period (e.g. 1 m.y., corresponding to a convergence rate of 8 cm y$^{-1}$) it would be possible to cool rocks at these great depths from 500 °C to 300–350 °C in the required period of $< \sim 3$ m.y. In this case rapid cooling to the relatively low temperatures implied by our MacArgon simulations could be achieved for rocks within a few kilometers of the thrust plane.

Metamorphic *P–T* data and structural observations support the thrusting model, and clearly the calculations above show that thrust movements could be a major contributing factor to the rapidity of cooling implied by our MacArgon models. Several lines of evidence imply that the EBD was thrust towards the north on $D_3$ shear zones, over the underlying units. Firstly the $M_2$ mineral paragenesis of the GSD is representative of lower pressures than that of the EBD, indicating that prior to $D_3$ the EBD was at deeper levels than the GSD. It is only during $D_3$ that the EBD rises to levels where the assemblage jadeite + quartz becomes unstable, whereas the GSD was at levels above the jadeite + quartz instability during $M_2$. Secondly, $D_3$ is more intense in the GSD whereas in the EBD $D_3$ shear zones tend to be localised. For instance there are some very large $D_3$ ductile shear zones in the GSD (e.g. the 400 m thick Faros shear zone) where intense $D_3$ strains have accumulated. There is also a significant degree of syn-to-post $D_3$ metamorphism in the GSD, which is lacking in the EBD. The longer and more protracted history of deformation and metamorphism in the GSD is consistent with the thrusting model, since the rocks in the underlying slab

will have remained at elevated temperatures for a longer period.

Although the modelling reported above does not consider erosional or tectonic denudation, the data above clearly imply that this is taking place during $D_3$ and subsequent events. During $D_3$, pressure in the EBD decreases by a total of 3–4 kbar (from $< \sim 14$ kbar). In the GSD, pressure during $M_3$ was 8–10 kbar, which indicates that erosional and/or tectonic denudation of the EBD must have taken place prior to this event (i.e. during $D_3$). Such effects can be considered in more complex thermal models, but to a first approximation, at such great depths in the Earth's crust, they are not likely to alter the conclusions reached in this section of the paper.

Younger $^{40}Ar/^{39}Ar$ apparent ages are obtained for rocks from deeper structural levels on Sifnos (i.e. from within the GSD) and apparent age spectra from the GSD show significant partial argon loss. Apparent $^{40}Ar/^{39}Ar$ age spectra from the highest structural levels (i.e. from within the EBD) have the oldest plateau ages and flat spectra. This data is consistent with cooling of the GSD during its later exhumation (from beneath the EBD) as the result of detachment faulting.

*Rapid cooling after a thermal pulse*

An alternative way that rapid cooling can be achieved at depth is if relatively cold rocks are subjected to a thermal pulse during which higher temperatures are only temporarily achieved. Rapid cooling can take place after the thermal pulse if the quantity of additional heat that has been introduced is relatively small, if the ambient temperatures were originally relatively low, and if the region of interest is spatially close to the source of the thermal pulse. Such a thermal pulse might take place, for example: (a) in the aureole of regionally significant igneous intrusions; (b) adjacent to a ductile shear zone that has radiated heat as the result of thermomechanical coupling (i.e. shear heating); (c) as a result of heat transported by migrating fluids; (d) from heat generated by metamorphic reactions.

We can illustrate the three constraints on the nature of the heat source (listed above) by exploring the case where a transient thermal event is caused by advective transport of heat during magmatism. The formulae provided by Turcotte & Schubert (1988) have been used to calculate the temperature history at varying distances from a sill of gabbro intruded at 1100 °C at depth in the crust. In each case shown in Fig. 11 the top of the sill is at 55 km, and the distances mentioned in the text reflect the distance from the top of the sill. Parameters used for conductivity, specific heat, and so on are those listed by Turcotte & Schubert (1988).

The first case considered (Fig. 11a) is that of a 2 km thick sill emplaced in a geothermal gradient of 7 °C km$^{-1}$. Temperatures up to ~2.5 km distance from the sill briefly exceed 500 °C and then the rocks rapidly cool. However even after 10 m.y. rocks <4 km from the sill are still at temperatures >400 °C, and thus too hot (at least according to our MacArgon simulations). It can be concluded that even a relatively low geothermal gradient such as 7 °C km$^{-1}$ produces ambient temperatures at ~50 km that are too high to allow rapid cooling below 350 °C. For the second case the temperature–time histories of rocks adjacent to a 5 km thick sill are considered. Again the sill is intruded at 1100 °C into a

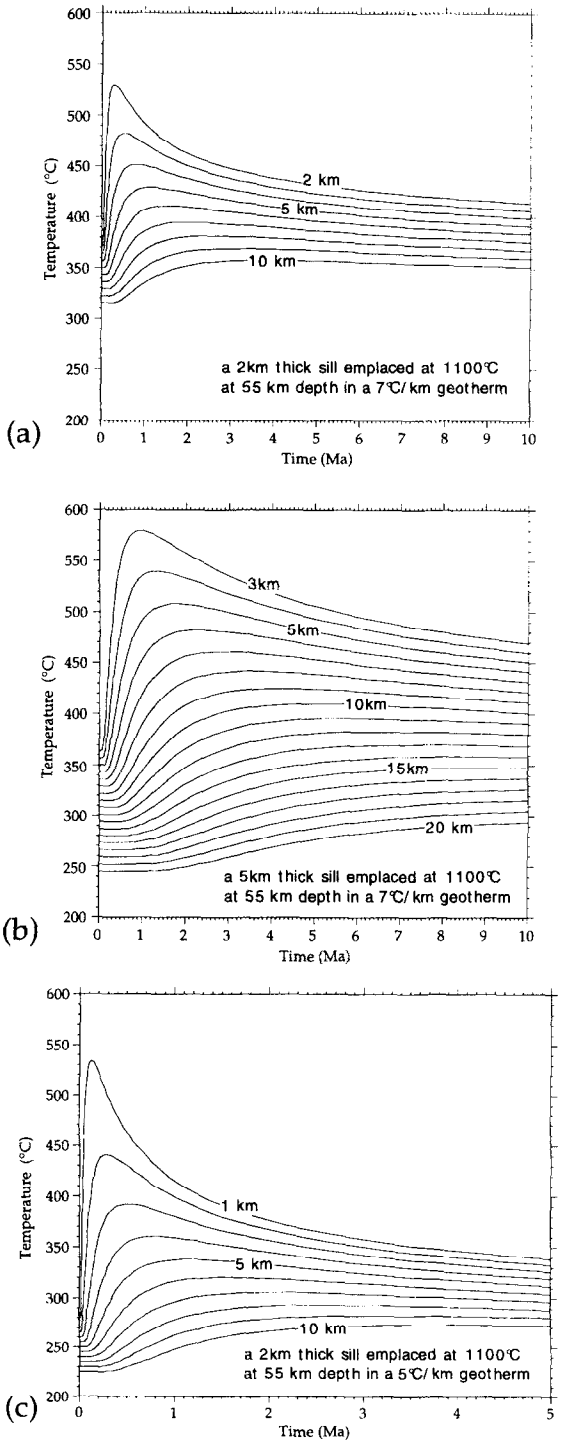


Fig. 11. Temperature–time histories for rocks in the vicinity of a thick basaltic sill intruded at 1100 °C at a depth of 55 km in crustal rocks with a geothermal gradient of 7 °C km$^{-1}$ (a) and (b) and 5 °C km$^{-1}$ (c). Temperature–time plot shows the heat wave as it passes through locations at specified distances from the intrusion front (locations are from 1 km to 20 km distant from the top of the intrusion). The sills used in (a) and (c) are 2 km thick, whereas in (b) a sill thickness of 5 km is assumed. Calculations based on Turcotte & Schubert (1988).

7 °C km$^{-1}$ geothermal gradient. Now rocks up to 5 km distance from the sill are raised above 500 °C during the thermal pulse, but after 10 m.y. temperatures are still in excess of 450 °C (Fig. 11b). The total quantity of heat introduced is too large and it will take much longer for temperatures to reduce. In the third case considered (see Fig. 11c) the geothermal gradient is abnormally low (i.e. 5 °C km$^{-1}$). A 2 km sill (as for Fig. 11a) is once again considered. In this case rapid cooling will take place, and temperatures will drop rapidly below ~350 °C. The obvious generalization from the three cases above is that rapid cooling will take place if small quantities of heat are introduced, if the ambient temperatures are initially very low, and if the rock mass we are considering is relatively close to the heat source responsible for production of the thermal pulse.

The hypothesis that an Eocene thermal pulse affected the high pressure–low temperature assemblages of Sifnos has merit because: (a) it allows explanation of the episodic nature of the porphyroblastic $M_2$ mineral growth event; (b) a thermal pulse would mechanically weaken the crust which might therefore more readily undergo deformation, allowing explanation of the $D_3$ event which begins during the late stages of $M_2$. However, if the peak conditions of metamorphism were achieved in a thermal aureole of a sill at depths <3 km distant from the rocks we are examining (e.g. see Fig. 11c), it is difficult to explain the apparent homogeneity in metamorphic grade that is observed within each structural domain (i.e. the EBD or the GSD). It is possible that we are examining the effects of a larger sill (e.g. Fig. 11b), in which case there would be a greater degree of homogeneity. But in this case we must explain rapid cooling as the result of tectonic processes as suggested in the previous section.

Short-lived episodes of mineral growth can occur as the result of a thermal pulse generated by the injection of regionally significant mantle derived igneous intrusions into the lower crust. Such intrusions could cause the upward propagation of a heat wave through the crust, triggering metamorphic reactions, and mechanically weakening the rocks. For this to be the explanation of the porphyroblastic overprint observed on Sifnos we must assume however that the initial geotherm was very low (< ~5 °C) possibly as the result of earlier thrust events which doubled or even quadrupled crustal and lithospheric thicknesses. We are also constrained to deal with sills of limited thickness (~ 2 km), within 1–2 km of the intrusive contact, and there is no evidence for the existence of such igneous intrusions.

It is possible that other sources of heat were involved. The advection of heat as the result of fluid migration might trigger metamorphic mineral growth, but significant volumes of fluid are necessary if a heat pulse is to result. An additional factor to be considered is the heat produced or absorbed by metamorphic reactions because if exothermic hydration reactions take place during $M_2$, a rise in temperature would result. Shear heating is another potential source of a thermal pulse, and this mechanism has the advantage that the heat is generated within the actual rock mass we are considering, or immediately adjacent to it. Once deformation stopped, temperatures would rapidly return towards those determined by the ambient conditions. However, a high level of deviatoric stress is required to allow a ductile shear zone to generate significant heat, and we observe microstructures typical of low deviatoric stress preserved in the $D_3$ ductile shear zones. Pressure shadows were filled by diffusive mass transfer processes, for example. Another difficulty is posed by timing relations, because our microstructural observations show that the period of blastic mineral growth precedes $D_3$, and mineral growth terminates during early $D_3$. If mineral growth is to be related to a thermal pulse caused by significant shear heating we would expect to see evidence for mineral growth during rather than prior to deformation.

### *Geodynamic significance of $M_2$*

Basement terrains in other parts of the Alpine collisional belt have been driven down to depths in excess of ~100 km early in their geological history, implying crustal thickening to at least 100–120 km (e.g. in the Doira Maira massif in the western Italian Alps). It is thus not difficult to explain an exceptionally low initial ambient geotherm as the result of transient relaxation after thrusting has doubled or even quadrupled the thickness of the continental lithosphere (see Fig. 10).

Convective thinning of the overthickened lithosphere may then have taken place, and this would lead to orogenic collapse (Platt & England 1993), as illustrated in Fig. 12. Consequent uplift of the asthenosphere may have resulted in partial melting, and any basaltic melts produced would rise and intrude the overlying continental crust. In such a way, a regional magmatic event may have been initiated, providing the ultimate source of a heat wave that propagated further upwards toward the surface. Such a transient thermal event might have triggered blastic growth during the $M_2$ metamorphism, followed by a major tectonic event ($D_3$) in the now thermally weakened crust.

## CONCLUSIONS

The following conclusions have been reached:

(1) The eclogite–blueschist domain on Sifnos has been subjected to a major porphyroblastic overprint ($M_2$) under epidote–blueschist facies conditions (> ~460 °C at < ~14 kbar) during the Eocene. Porphyroblasts of glaucophane, white mica, epidote and garnet overgrew higher pressure omphacite- and jadeite-rich assemblages. A major period of deformation ($D_3$) commenced during the last stages of $M_2$.

(2) Stepped apparent age spectra result from MacArgon simulations that use the $P$–$T$–$t$ paths published by Wijbrans *et al.* 1990, 1993. These do not resemble the apparent age spectra measured from Sifnos.

(3) Flat apparent age spectra as measured by Wijbrans *et al.* (1990) from the EBD can be replicated by

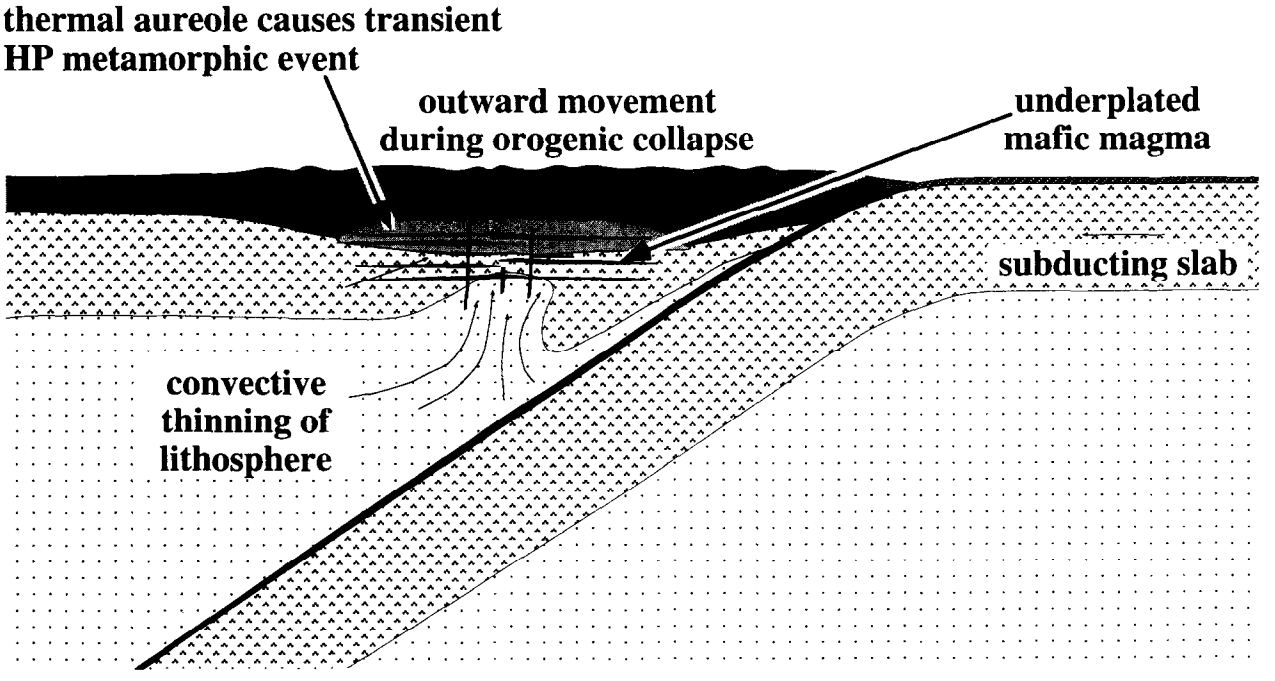


Fig. 12. Schematic illustration of a tectonic model to explain the history of deformation and metamorphism proposed in this paper. Continental collision is followed by orogenic collapse. Convective thinning of the lithosphere leads to asthenospheric upwelling, and partial melting results. Basaltic magmas rise and intrude the lower crust. These cause thermal pulses which give rise to transient episodes of regional metamorphism, at the same time as they thermally weaken the continental crust. A major episode of tectonic activity then follows each metamorphic event.

MacArgon simulations based on the diffusion parameters for phlogopite if the eclogite–blueschist domain is cooled rapidly at ~42 Ma from peak temperatures (~500 °C) to <~350 °C at rates >~50 °C m.y.$^{-1}$. Cooling must continue after the period of rapid temperature decrease otherwise significant argon loss will take place.

(4) Cooling rates that exceed ~50 °C m.y.$^{-1}$ imply that the apparent ages obtained from the eclogite–blueschist domain by Wijbrans *et al.* (1990) approximate the age at which $M_2$ terminated and $D_3$ commenced (~42 Ma), and that the EBD cooled rapidly at rates >~50 °C m.y.$^{-1}$ to below ~350 °C during $D_3$.

(5) MacArgon simulations suggest that cooling in the greenschist domain on Sifnos started at ~32 Ma at rates of ~50 °C m.y.$^{-1}$ and rapid cooling continued until temperatures were <~350 °C. The simulations also imply that the GSD has not been significantly affected by a Miocene thermal pulse. Significant partial argon loss would be observed in the measured apparent age spectra if temperatures had exceeded ~350 °C for more than ~2 m.y.

(6) The link between $M_2$ and $D_3$ suggests that if a thermal pulse did trigger an episode of regional metamorphism, rapid cooling after this event may have been directly related to tectonism (e.g. thrust juxtaposition of the EBD against cooler more surficial levels of the crust).

(7) Rapid cooling can be achieved in the lower part of an upthrusted block as the result of its juxtaposition against cooler rocks from shallower crustal levels. The geotherm must be ~10 °C km$^{-1}$ if the peak temperature of ~500 °C at 14 kbar is to be achieved. In this case, rocks within 5–10 km of the thrust plane can cool to ~350 °C in 1–2 m.y. after they are juxtaposed against surficial rocks as the result of instantaneous downthrusting involving a relative displacement of at least 80 km.

(8) Rapid cooling can also result after a thermal pulse, independently of the effects related to thrust juxtaposition, but only if the initial ambient geothermal gradient was very low (<~5 °C km$^{-1}$). If rapid cooling is to occur, only a limited additional input of heat can take place, and the heat source must be relatively close (i.e. within 1–2 km) of the rocks affected by the thermal pulse.

*Acknowledgements*—The authors acknowledge support from Australian Research Council grant to study the processes of 'Continental Extension Tectonics'. The support of the I.G.M.E. in Athens is acknowledged, in particular Dr Vaios Avdis, for his hospitality and advice. The research in this paper was made possible by the people of Sifnos, in particular Dimitri and Maria Koukoletsos, and Maria and Kostas Katzlieri. Thorough reviews and thoughtful comments provided by Andrew Barnicoat, Liz Schermer, and Richard Norris were particularly helpful to the authors.

## REFERENCES


Altherr, R., Schliestedt, M., Okrusch, M., Seidel, E., Kreuzer, H., Harre, W., Lenz, H., Wendt, I. & Wagner, G. A. 1979. Geochronology of high pressure rocks on Sifnos (Cyclades, Greece). *Contr. Miner. Petrol.* **70**, 245–255.

Altherr, R., Kreuzer, H., Wendt, I., Lenz, H., Wagner, G. A., Keller, J., Harre, W. & Höhndorf, A. 1982. A Late Oligocene/Early Miocene high temperature belt in the Attic–Cycladic crystalline complex (SE Pelagonian, Greece). *Geol. Jb.* **E23**, 97–164.

Andersen, T. B., Osmundsen, P. T. & Jolivet, L. 1994. Deep crustal fabrics and a model for the extensional collapse of the southwest Norwegian Caledonides. *J. Struct. Geol.* **16**, 1191–1204.

Avigad, D. 1993. Tectonic juxtaposition of blueschists and greenschists in Sifnos Island (Aegean Sea) — implications for the structure of the Cycladic blueschist belt. *J. Struct. Geol.* **15**, 1459–1469.

Avigad, D. & Garfunkel, Z. 1991. Uplift and exhumation of high pressure metamorphic terrains: the example of the Cycladic blueschist belt (Aegean Sea). *Tectonophysics* **188**, 357–372.

Avigad, D., Matthews, A., Evans, B. W. & Garfunkel, Z. 1992. Cooling during exhumation of a blueschist terrane: Sifnos (Cyclades), Greece. *Eur. J. Mineral.* **4**, 619–634.

Berman, R. G. 1988. Internally consistent thermodynamic data for minerals in the system $Na_2O$–$K_2O$–CaO–MgO–FeO–$Fe_2O_3$–$Al_2O_3$–$SiO_2$–$TiO_2$–$H_2O$–$CO_2$. *J. Petrology* **29**, 445–552.

Berman, R. G. & Perkins, E. H. 1987. GEO-CALC: software for the calculation and display of temperature–pressure–composition phase diagrams. *Am. Miner.* **72**, 861–862.

Coyle, D. A. and Wagner, G. A. 1994. Fission track investigation in sphene from the KTB deep drilling program (Germany): post-Permian cooling history and anisotropic annealing. *Abstracts of the 8th International Conference on Geochronology, Cosmochronology and Isotope geology* (edited by M. A. Lanphere, G. B. Dalrymple and B. D. Turrin) U.S.G.S. Circular 1107, 69.

Davis, E. N. 1966. Der Geologische Bau der Insel Sifnos. *Geol. Geophys. Res. Athens* **10**, 161–220.

Dewey, J. F. 1988. Extensional collapse of orogens. *Tectonics* **7**, 1123–1139.

Diez Balda, M. A., Martinez Catalan, J. R. & Ayarza Arribas, P. 1995. Syn-collisional extensional collapse parallel to the orogenic trend in a domain of steep tectonics: the Salamanca detachment zone (Central Iberian zone, Spain). *J. Struct. Geol.* **17**, 163–182.

England, P. C. & Holland, T. J. B. 1979. Archimedes and the Tauern eclogites: the role of buoyancy in the preservation of exotic eclogite blocks. *Earth Planet. Sci. Lett.* **44**, 287–294.

Evans, B. W. 1986. Reactions among sodic, calcic, and ferromagnesian amphiboles, sodic pyroxene, and deerite in high-pressure metamorphosed ironstone, Sifnos, Greece. *Am. Miner.* **71**, 1118–1125.

Evans, B. W. 1990. Phase relations of epidote–blueschist. *Lithos* **25**, 3–23.

Giletti, B. J. 1974. Studies in diffusion I: Argon in phlogopite mica. In *Geochemical Transport and Kinetics* (edited by A. W. Hofmann, B. J. Giletti, H. S. Yoder and R. A. Yund), 107–115. Carnegie Inst. Washington, Publcn 634.

Gleadow, A. J. W. 1978. Anisotropic and variable track etching characteristics in natural sphenes. *Nuclear Track Detect.* **2**, 105–117.

Gleadow, A. J. W. & Lovering, J. F. 1978. Thermal history of granitic rocks from western Victoria: a fission track dating study. *J. geol. Soc. Aust.* **25**, 323–340.

Holland, T. J. B. & Powell, R. 1985. An internally consistent dataset with uncertainties and correlations: data and results. *J. Metamorph. Geol.* **3**, 343–370.

Houseman, G. A. & McKenzie, D. P. 1981. Convective instability of a thickened boundary layer and its relevance for the thermal evolution of continental convergent belts. *J. geophys. Res.* **86**, 6115–6132.

Lee, J. K. W., Onstott, T. C., Cashman, K. V., Cumbest, R. J. & Johnson, D. 1991. Incremental heating of hornblende in vacuo: implications for $^{40}Ar/^{39}Ar$ geochronology and the interpretation of thermal histories. *Geology* **19**, 872–876.

Lister, G. S. and Baldwin, S. L. 1996. Modelling the effect of arbitrary *P–T–t* histories on argon diffusion in minerals using the MacArgon program for the Apple Macintosh. *Tectonophysics* **253** 83–109.

Lister, G. S., Banga, G. & Feenstra, A. 1984. Metamorphic core complexes of Cordilleran type in the Cyclades, Aegean Sea, Greece. *Geology* **12**, 221–225.

Lister, G. S., Boland, J. N. & Zwart, H. J. 1986. Step-wise growth of biotite porphyroblasts in pelitic schists of the western Lys-Caillaouas massif (Pyrenees). *J. Struct. Geol.* **7**, 543–562.

Matthews, A. & Schliestedt, M. 1984. Evolution of the blueschist and greenschist facies rocks of Sifnos, Cyclades Greece. *Contr. Miner. Petrol.* **88**, 150–163.

McDougall, I. and Harrison, T. M. (1988) *Geochronology and Thermochronology by the $^{40}Ar/^{39}Ar$ Method.* Oxford University Press.

Miller, E. L., Calvert, A. T. & Little, T. A. 1992. Strain-collapsed metamorphic isograds in a sillimanite gneiss dome, Seward Peninsula, Alaska. *Geology* **20**, 487–490.

Naeser, C. W. & Faul, H. 1969. Fission track annealing in apatite and sphene. *Geophys. Res.* **74**, 705–710.

Okrusch, M., Seidel, E. & Davis, E. N. 1978. The assemblage jadeite–quartz in the glaucophane rocks of Sifnos (Cycladic Archipelago, Greece). *N. Jahrb Mineral Abh.* **132**, 284–308.

Platt, J. P. & England, P. C. 1993. Convective removal of lithosphere beneath mountain belts: thermal and mechanical consequences. *Am. J. Sci* **293**, 307–336.

Platt, J. P. & Lister, G. S. 1985. Structural history of high-pressure metamorphic rocks in the southern Vanoise massif, French Alps, and their relation to Alpine tectonic events. *J. Struct. Geol.* **7**, 19–35.

Powell, R. & Holland, T. J. B. 1988. An internally consistent dataset with uncertainties and correlations: 3. application to geobarometry, worked examples and a computer program. *J. Metamorph. Geol.* **6**, 173–204.

Raouzaios, A. 1993. Deformation and metamorphism on the island of Sifnos, Cyclades, Greece: tectonic implications for the exhumation of a coherent eclogite–blueschist terrain. Unpublished MSc. prelim. thesis, Monash University, Melbourne, Australia.

Raouzaios, A., Lister, G. S. & Foster, D. 1996. Oligocene exhumation and metamorphism of eclogite–blueschists from the island of Sifnos, Cyclades, Greece. *Geol. Soc. Australia, Abstracts* **41**, 358.

Ridley, J. 1984. Listric normal faulting and the reconstruction of the syn metamorphic structural pile of the Cyclades. In: *The Geological Evolution of the Eastern Mediterranean* (eds J. E. Dixon & A. H. F. Robertson) *Geol. Soc. Spec. Publ.* **17**, 755–761.

Robbins, G. A. 1972. Radiogenic argon diffusion in muscovite under hydrothermal conditions. Unpublished MSc thesis, Dept Geol. Sci., State University of New York at Albany.

Schliestedt, M. 1986. Eclogite–blueschist relationships as evidenced by mineral equilibria in the high-pressure metabasic rocks of Sifnos (Cycladic Islands), Greece. *J. Petrology* **27**, 1437–1459.

Schliestedt, M. & Matthews, A. 1987. Transformation of blueschist to greenschist facies rocks as a consequence of fluid infiltration Sifnos (Cyclades) Greece. *Contr. Miner. Petrol.* **97**, 237–250.

Turcotte, D. L. and Schubert, G. 1988. *Geodynamics: Application of Continuum Physics to Geological Problems.* Wiley, New York.

Vernon, R. H. 1976. *Metamorphic Processes, Reactions and Microstructure Development.* Allen and Unwin, London.

Vissers, R. L. M. 1992. Variscan extension in the Pyrenees. *Tectonics* **11**, 1369–1384.

Voorhoeve, H. & Houseman, G. A. 1988. The thermal evolution of lithosphere extending on a low-angle detachment zone. *Basin Research* **1**, 1–9.

Wijbrans, J. R. & McDougall, I. 1986. $^{40}Ar/^{39}Ar$ dating of white micas from an Alpine high pressure metamorphic belt on Naxos (Greece): the resetting of the argon isotopic system. *Contr. Miner. Petrol.* **93**, 187–194.

Wijbrans, J. R. & McDougall, I. 1988. Metamorphic evolution of the Attic Cycladic metamorphic belt on Naxos (Cyclades, Greece) utilising $^{40}Ar/^{39}Ar$ age spectrum measurements. *J. Metamorph. Geol.* **6**, 571–594.

Wijbrans, J. R., Schliestedt, M. & York, D. 1990. Single grain argon laser probe dating of phengites from the blueschist to greenschist transition on Sifnos (Cyclades, Greece). *Contr. Miner. Petrol.* **104**, 582–594.

Wijbrans, J. R., van Wees, J. D., Stephenson, R. A. & Cloetingh, S. A. P. L. 1993. Pressure–temperature–time evolution of the high pressure metamorphic complex of Sifnos, Greece. *Geology* **21**, 443–446.

Zwart, H. J. 1979. The geology of the central Pyrenees. *Leidse Geologische Mededelingen* 50, 74 pp.